1 **Nitrogen-loads to streams across two different riparian zones (crop field and**

2 **wetland): Importance of bypass flow and subsurface removal processes.**

3

4 Mads Steiness[1], Søren Jessen[1], Sofie G.W. van 't Veen[1,2], Tue Kofod[1,3], Anker Lajer Højberg[4] and

5 Peter Engesgaard[1*]

6

Key points:

- Nitrate-load to stream controlled by draining practice, ratio of riparian to catchment area, and depth to redox interface.
- Hotspots allow complete denitrification with pyrite and/or organic matter, but N-load to stream remains high due to bypass flow via drain management structures.
- A conceptual model for buffer efficiency based on bypass flow fraction and Damköhler number is presented.

15 [1] Department of Geosciences and Natural Resource Management, University of Copenhagen, 1350

16 Copenhagen, Denmark; mast@ign.ku.dk (M.S.); sj@ign.ku.dk (S.J.); pe@ign.ku.dk (P.E.)

17 [2] Department of Bioscience, Aarhus University, 8600 Silkeborg, Denmark; svv@bios.au.dk (S.V.)

18 [3] Danish Water Works, Solrød Center 20C, 2680 Solrød Strand, Denmark; tko@danskevv.dk

19 [4] Geological Survey of Denmark and Greenland, Department of Hydrology, 1350 Copenhagen,

20 Denmark; alh@geus.dk (A.H.)

21 [*] Corresponding author (PE, ORCID, 0000-0002-5925-8757)

Abstract

23 N-loads from subsurface, drains, and groundwater-fed surface (bypass) flows via two riparian zones

24 (crop field and wetland) to a second order stream were investigated by sampling of shallow and

25 deep groundwater on both sides and monthly measurements of flows from springs, drains, and

26 stream including water quality (nitrate). A push-pull test in the crop field gave estimates of first-

27 order denitrification rate (0.23 day^{-1}). Reactive transport modelling evaluated observations of water

28 chemistry and denitrification processes in the groundwater below the crop field showing that nitrate

29 was completely removed by denitrification with pyrite in the aquifer (model rates of 0.6–2.5 mmol

30 NO_3 L^{-1} yr^{-1}). A drain in the crop field routed approximately 10% (bypass) of the regional

31 groundwater inflow to the stream. Buffer efficiency was high at 90%. The wetland on the other side

32 of the stream hosts several locations of focused nitrate-rich groundwater-fed spring discharge,

33 predominantly through a non-maintained drainage system of drainpipes and ditches with bypass

34 accounting for 59% of the regional flow input. Nitrate was completely removed in groundwater by

35 denitrification with dissolved organic matter in shallow groundwater. The regional inflow and N

36 load to the wetland is amongst the highest recorded and data shows that the N load to the stream is

37 very high. The buffer efficiency ranged from 45–83% depending on if all springs contributed to the

38 stream or only the two with visible outflow. A conceptual model for nitrate removal efficiency as a

39 function of Damköhler number and percent bypass flow is proposed.

40

41 Plain language summary

42 Riparian zones connect agricultural catchments to streams and are important for intercepting and

43 removing nitrate. The effects of bypass flow due to overland flow from natural springs, seeps or

44 through drainpipes are often overlooked. We developed a generic conceptual model for riparian

45 buffer efficiency (ratio of how much nitrate is removed relative to the input) based on detailed field

46 investigations in two contrasting riparian zones (crop field and wetland). One would think that the

47 crop field would be the main source of nitrate to the stream, but it is not. Input of water and nitrate

48 to the stream was much higher on the wetland side, where nitrate-containing groundwater was

49 funneled through the small wetland. The inflow of water was so high that numerous small natural

50 springs and seeps were present and, historically, a network of ditches and drainage pipes were

51 installed to keep the wetland relatively dry. Bypass flow is high (59%) and data shows some of the

52 highest recorded nitrate loads to a stream. Complete removal of nitrate in groundwater flowing

53 through both riparian zones was observed. Buffer efficiency is high with 90% on the crop side and

54 45–83% on the wetland side.

55

58

59

1. Introduction

Nutrients applied in connection with agriculture may enter the groundwater and ultimately end up in streams. Riparian lowlands have shown to hold the potential to significantly decrease nitrate (NO_3) concentrations in groundwater flowing from uplands to streams (Peterjohn and Correll 1984, Sabater et al. 2003, Vidon and Hill 2005, Hill 2018, 2019). Restoration of wetlands can therefore be an important mitigation method for increasing NO_3 removal (Audet et al. 2020). The removal of NO_3 in the riparian lowland is recognized to occur from biological uptake and denitrification reactions under anoxic conditions (Hill 2019). Denitrification has been demonstrated to be the main removal process of NO_3 in riparian aquifers (Hill 2018, 2019), although additional processes such as plant uptake can be more important than denitrification (Lutz et al., 2020). Denitrification can occur with organic matter as an electron donor (heterotrophic denitrification), but can also occur with inorganic sources via the oxidation of ferrous iron (Fe^{2+}) and reduced sulfur (S; autotrophic denitrification) (Korom 1992).

73

Hydrological flow paths and nitrate transport through the riparian lowland are controlled by the inherent heterogeneity, which to a large degree also controls the N-removal efficiency and the occurrence of so called "hot spots" (McClain et al. 2003) for denitrification (e.g., Devito et al. 2000). Typologies and conceptual classification systems for upland hydrological connectivity and deep, shallow or bypassing flow paths have been proposed based on field studies to characterize groundwater-stream interaction and potential N-removal in riparian lowlands (Hill 1996, Vidon and Hill 2004, Dahl et al. 2007, Jencso et al. 2009, Noij et al. 2012).

81

Hydrologic connectivity (e.g. subsurface flow, groundwater-fed surface flow, drainage) across the riparian lowland influences not only the N-transporting flow paths, but also the soil moisture conditions and redox potentials within N-removal zones of the lowland, which in turn may affect the NO_3 buffering efficiency of riparian lowlands (Burt et al. 2002, Puckett and Hughes 2005). In this study, we focus on gaining streams and not streams or rivers that infiltrate to groundwater (see e.g. Lutz, 2020). The magnitude and variance of the upland groundwater- and solute fluxes fed to riparian lowlands are controlled by size- and transmissivity of upland aquifers (Vidon and Hill 2004). Large and thick regional aquifers provide riparian lowlands with a relatively steady input of

90   groundwater (Hill 1996). The groundwater loading to a lowland is sometimes referred to as the

91   hydraulic loading by which the riparian zone-to-catchment area ratio becomes important (Audet et

92   al. 2020; Petersen et al. 2020). With deeper aquifers, studies have shown that observed decreases in

93   NO_3 concentrations across riparian zones may be due to dilution, instead of removal by

94   denitrification, as mixing of young, shallow nitrate-rich groundwater with older, deeper nitrate-free

95   groundwater can occur (Puckett and Cowdery 2002, Puckett 2004, Hefting et al. 2006).

96

97   Likewise, riparian lowland hydrogeology may allow bypassing of nitrate-rich groundwater rather

98   than diffuse flow through the riparian aquifer, which in turn affects nitrate removal efficiency (Burt

99   et al. 1999, Puckett 2004). Generally, a thick and permeable riparian aquifer allows the flow of

100 regional groundwater of varying ages to bypass the nitrate reducing zones near organic-rich top

101 layers (Hill 1996, Devito et al. 2000, Puckett and Hughes 2005). In shallow riparian aquifers the

102 fraction of bypassing water in the subsurface may decrease depending on how much groundwater-

103 fed surface flow is generated. This is also observed for low-permeable riparian aquifers, which

104 favor the creation of seeps and springs at the break in slope generating surface flow, that may form

105 rivulets discharging directly to the stream as overland flow or re-infiltrate to the riparian aquifer

106 (Brüsch and Nilsson 1993, Shabaga and Hill 2010).

107

108 Artificial drainage of riparian lowlands to make them usable for agricultural production is common

109 in agricultural lowland catchments and can increase bypassing of nitrate-rich groundwater (Puckett

110 2004). Ditches and subsurface drains provide conduits for water to move rapidly through the

111 riparian system, minimizing the riparian lowlands potential nutrient attenuation. Hence,

112 manipulation of the hydrologic flow regimes alters the physical character of riparian systems by

113 routing water directly from the hillslope to the stream, bypassing the denitrifying zones within the

114 entire riparian lowland, and this accordingly becomes manifested in the water quality of adjacent

115 streams.

116

117 Few studies have evaluated the combined influence of natural groundwater seeps/springs and

118 drainage on how N-loads in riparian lowlands partitions between direct groundwater discharge and

119 bypass flow to the stream. For example, Audet et al. (2020) surveyed more than 20 restored

120 wetlands in Denmark, but only measured surface inlets and outlets, and not groundwater. Petersen

et al. (2020) measured and/or estimated all flow paths (subsurface, drains, surface) in riparian lowlands of clayey till catchments. Not surprisingly for this type of geological environment, groundwater fluxes to and from the lowlands were much smaller than drain fluxes. Shabaga and Hill (2010) demonstrated how upwelling groundwater was transported 100 m along rivulet-pipe networks in the upslope parts of their field sites, with little nitrate removal, converging into diffusive flow and increased nitrate removal in the downslope parts. The rivulet-pipe networks are shallow natural macropore systems that provided conduits for water and solutes across the riparian zones acting similar to a drain system. Clausen et al. (1993) measured nitrate fluxes in precipitation, overland flow, soil solution, groundwater and stream flow in a riparian area and found that the majority of the N flux took place via groundwater, but with little retention by for example denitrification. The importance of groundwater-fed surface flow bypassing (by natural or anthropogenic causes) riparian N removal zones on the delivery of nitrate to streams is therefore still not fully understood.

The aim of the present study is; (1) to examine how bypass flow and direct groundwater discharge affect nitrate delivery to a second-order channelized stream located in western Denmark and (2) to develop a simple model for nitrate removal efficiency as a function of two important parameters; the Damköhler number and the percent bypass flow. The Damköhler number expresses the ratio of transport to reaction time scales. Percent bypass flow is the sum of all water not diffusively flowing through the riparian aquifer to the stream, i.e., flow in drains and all groundwater-fed surface flows (rivulets, diffuse surface flow). It is a comparative study examining flow and water quality of two riparian zones on opposite sides of the stream. On the northeast side, the riparian zone comprises a crop field flanked by a buffer zone and with a small watershed. On the southwest side, the riparian zone is a wetland receiving groundwater inflow from a much larger watershed resulting in many seeps and which has a poorly functioning drainage system. Nitrate loadings from different flow paths to the stream and their impact on stream water quality are examined. Further, mechanisms responsible for removal of nutrients are studied using water quality data, a push-pull test, and geochemical modelling. We believe the field site to be characteristic to many other lowland riparian valleys and that the results therefore are applicable to many other areas.

2. Study site

The study was conducted in a riparian lowland situated in the upper part of Holtum catchment in the central part of Jutland, Denmark (Steiness et al. 2019). Holtum stream is characterized as a perennial second-order stream flowing from east to west. The surficial aquifer mainly consists of late Weichselian sandy outwash deposits and clayey tills, underlain by Miocene deposits of clay and sand. The shallow aquifer is partially unconfined/confined. Land use is dominantly agriculture (54%), forest (32%), and urban (14%) areas (Karan et al. 2013). Means of annual precipitation and actual evapotranspiration in the catchment were estimated to 984 and 510 mm/yr, respectively (Sebok et al. 2016).

The 3-m wide stream at the field site was channelized likely prior to the 1850s. The average discharge at the field site in 2017 was ~0.3 m^3 sec^{-1} (Steiness et al. 2019). On the northeastern side (the crop side), the riparian lowland comprises a 35-meter-wide grass buffer zone between the stream bank and a 145-meter-wide agricultural crop field (Figure 1A and 1B). The area is ~2.3 ha. A drainage-pipe (DR) discharges shallow groundwater from a small surface depression in the agricultural field and directly into the stream. Average drain pipe discharge in 2017 was 3.2×10^{-4} m^3 s^{-1} (~20 L/min, Steiness et al. 2019).

The southwestern side (the wetland side) is an 80-meter-wide wetland functioning as a cow pasture. In the wetland (~1.3 ha), six overland discharge systems are located; two springs (S1 and S2), an overflowing drainage well (DW), an overflow pipe from a pond (PO), a ditch (DI) and a small rivulet (RI), Figure 1B (from now on collectively termed *springs*). The DI and RI discharge directly to the stream. A submerged drain in the stream is also located at the bend of the stream to the southeast (Figure 1B). Several ditches (D1–D3) also drain the wetland downstream of the study site, Figure 1A. Most of the surface water systems were likely installed to drain the wetland. However, whether S1 and S2 are man-made installations (e.g. broken drain pipes that generate overland flow) or natural springs is not clear. Observed artesian conditions generating a natural diffuse seepage in the hill slope area above the pond were observed in the wetland. Steiness et al. (2019) found that the average total discharge from the springs was 2.7×10^{-3} m^3 s^{-1}. Direct groundwater discharge through the streambed (2.08×10^{-4} m^3 s^{-1}) was 13 times less.

The riparian lowland comprises a sandy aquifer with interbedded gravel lenses. The aquifer is unconfined on the crop side of the stream, whereas the aquifer under the wetland is partially

182   confined by a peat layer. The hydraulic conductivity of the riparian sandy aquifer ranges from

183   0.1–50 m day^{-1} with an average of 14 m day^{-1} (Steiness et al. 2019). Groundwater is flowing to the

184   stream from both the crop and wetland sides (Figure 1C).

185

186   The immediate upland northeast of the crop site is covered by a coniferous forest extending to the

187   topographical border of the catchment. The topographical catchment area is ~5 ha (based on a GIS

188   analysis). The upland to the south and southwest of the wetland site is comprised mainly of arable

189   land, with minor forested areas primarily on the hillslopes. The topographical catchment area of ~25

190   ha (based on a GIS analysis) is 5 times larger than north of the stream. The crop field/wetland to

191   upland area ratios are therefore 47% and 5%, respectively.
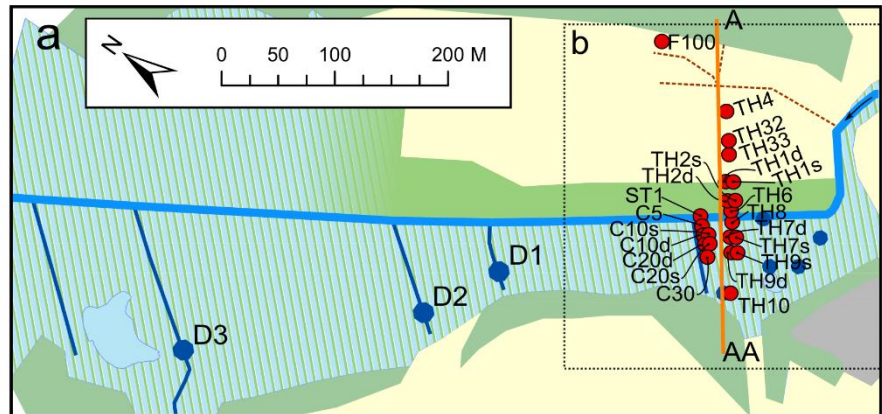
Legend (a & b)

Agriculture
Buffer strip
Forest
Wetland
Surface water
Urban
60 — Topo. [m.a.s.l.]
Springs
Piezometer
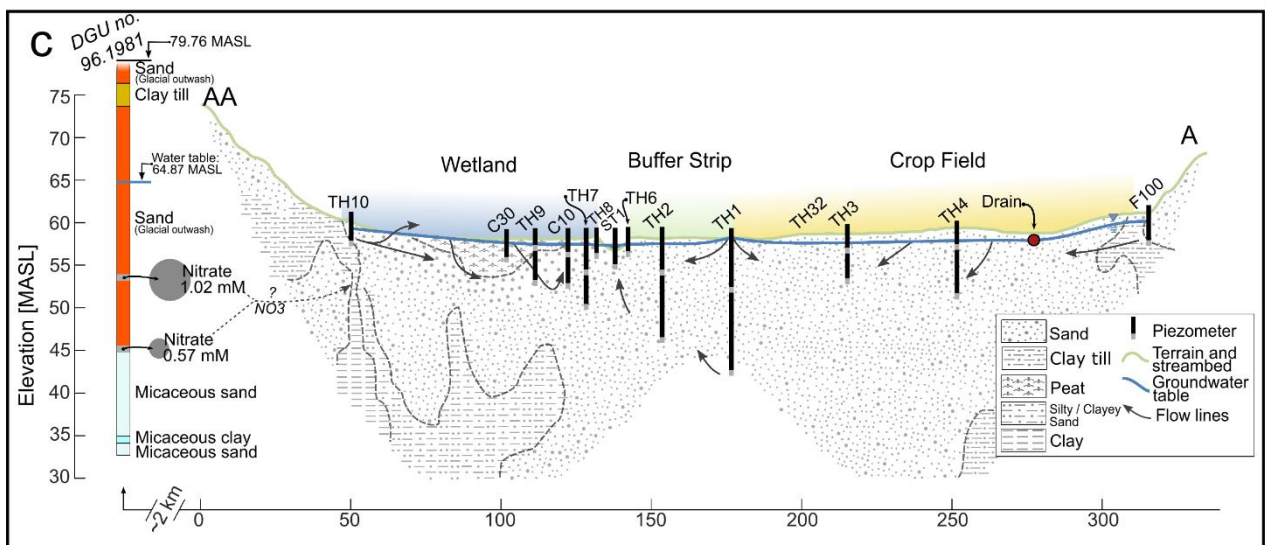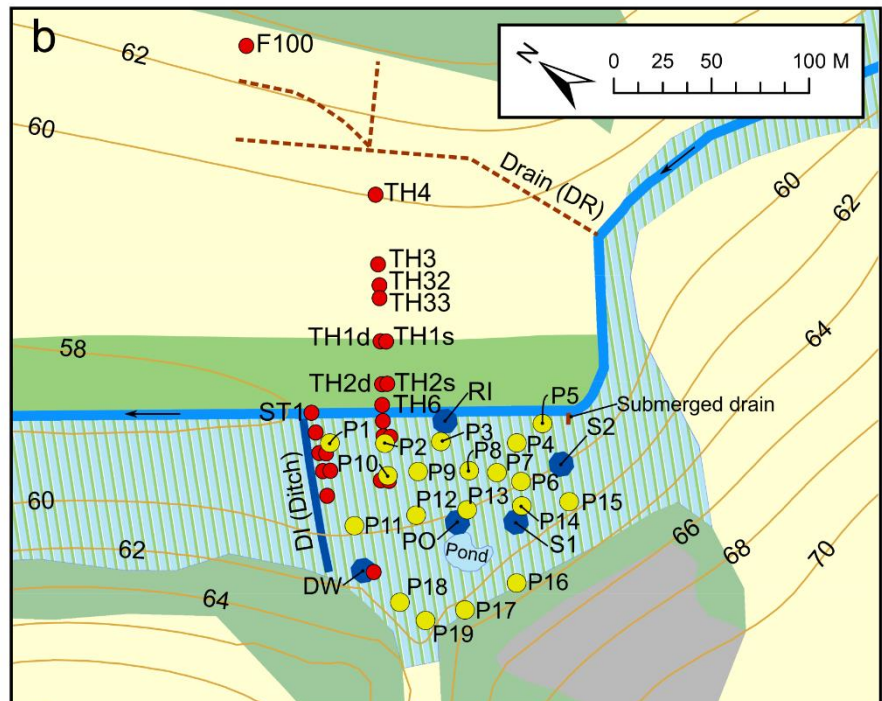Mini piezometer
Stream
Ditch
Drain

192

Figure 1. Field site in Holtum catchment in the central part of Jutland, Denmark (32 U., 520513 m E, 6204065 m N). (a) Northeast of the stream, a 35-meter wide grass-buffer separates the stream and the crop field. Southwest of the stream, a wetland extends to the hillslope. Several ditches are connected to the stream downstream of the field site (D1, D2 and D3). (b) In the riparian wetland six "springs" are located (DI, DW, PO, RI, S1 and S2) representing bypass flow paths. In addition, a drain (DR) is located under the crop field. c) Cross-section showing the geology of the riparian aquifer and groundwater flow directions. Groundwater flows diffusively through the aquifer towards the stream (Steiness et al. 2019). However, notice the small water mound at well TH1. A national monitoring well (96.1981) is shown with average nitrate concentrations (1990-2018) at two filters (see also Appendix A).

3. Materials and methods

Instrumentation includes 23 piezometers (Figure 1A and 1B) screened at different depths, installed at different times from 2015 to early 2017 (Poulsen et al. 2015, Steiness et al. 2019). All piezometers are equipped with a 9 cm screen near the bottom. Eight piezometers shown in Figure 1 are nested, consisting of a shallow (piezometer name followed by an *s*) and a deep (piezometer name followed by a *d*) piezometer screen. These are TH1, TH2, TH3, TH4, TH7, TH9, C10 and C20.

3.1 Water sampling and analysis

Monthly water sampling was carried out between January 2017 and January 2018 from the springs in the wetland, Holtum stream, and the drain (see Figure 1A and 1B; no samples were collected in July 2017). Piezometers were sampled on multiple occasions in the period from November 2015 up until October 2017. In addition, a campaign was conducted in June 2017 to sample the shallow groundwater underneath the peat layer in the wetland. Nineteen point-samples were collected using 'mini' piezometers (Figure 1B) (Steiness et al. 2019). The mini-piezometers had an inner diameter of 0.5 cm and were equipped with a 5 cm long screen. They were hammered to the desired depth just below the peat layer. Sampling followed the same procedure as described below for the regular piezometers.

222   Samples from D1, D2, and D3 were collected in June 2017. The submerged drain was sampled at

223   two separate occasions; in May 2017 and in January 2018. Also, several piezometers were sampled

224   at multiple depths during installation: TH1d, TH2d, TH3, TH4, TH7d and TH9d.

225

226   Water samples for major an- and cations (Cl, SO_4, F, Br, NO_3, NO_2, PO_4, NH_4, Na, K, Ca and Mg),

227   sulfide (H_2S), reduced iron (Fe^{2+}), and alkalinity were collected from piezometers (groundwater),

228   groundwater-fed springs, surface water (D1, D2, D3 and Holtum stream) and from the drain on the

229   crop side (DR).

230

231   Groundwater samples were collected using a peristaltic pump and a flow-cell (WTW Oxi 3310 IDS

232   and HACH HQ30). Water sampling commenced, when flow-cell values of dissolved oxygen,

233   temperature, pH, and electrical conductivity were stable. For sampling of springs, surface, and drain

234   water, the electrodes were immersed directly into the running water. Water samples were in all

235   cases taken with 60 mL polyethylene syringes and immediately filtered in the field through a 0.20

236   µm cellulose acetate syringe filter (Sartorius Minisart®). To avoid oxygenation of Fe^{2+} during

237   filtration (and consequent loss of PO_4 and other ions adsorbing to Fe oxides) the syringe filter was

238   vacuumized to remove oxygen. A vaccum was applied immediately prior to sample filtration using

239   a combination of a dry 60 mL syringe and two three-way valves. Samples for cations were acidified

240   with 1 vol% 1 M HNO_3 and stored in a refrigerator. Anion samples were stored frozen. Anions and

241   cations were analyzed by ion chromatography (Metrohm 820-IC Separation Center with 819-IC

242   Detector). Samples for Fe^{2+} and H_2S analysis were collected in separate 3 mL vials prefilled with,

243   respectively, 0.1 mL of ferrozine solution or 0.3 mL 10 wt% Zn acetate. The Fe^{2+} and H_2S

244   concentrations were measured spectrophotometrically in the laboratory following the procedures by

245   Stookey (1970) and Cline (1969), respectively. Samples for alkalinity (also filtered) were collected

246   in 100 mL acid-washed amber glass bottles and analyzed using endpoint titration on a Metrohm

247   autotitrator.

248

249   3.2 Pyrite measurements

250   In September 2016, cores were extracted from under the crop field near piezometers TH32 and

251   TH3.3, Figure 1B. Intact cores were collected from 0−1 and 1−2 m below surface (MBS) using

252 percussion drilling combined with a 1 m liner sampler. The core ends were sealed with caps and
253 additional tape and stored at −18°C to minimize oxidization until analysis.

254

255 Five subsamples of sediment with a sample spacing of 0.1 m from depths 1.6–2 MBS were freeze-
256 dried, homogenized (ring-mill grounded) and analyzed. The chromium reducible sulfur (CRS)
257 method was used to measure reduced inorganic sulfur compounds of the material sample following
258 Canfield et al. (1986). The chromium reducible sulfur in this study is mainly presumed to stem from
259 pyrite. From each subsample, 2 g of the dry and homogenized sediment was added to a mixed
260 solution of chromium(II) and concentrated hydrochloric acid (6 M HCl) in an inert N_2 atmosphere.
261 Throughout a 60 min boil, the liberated H_2S from the reduction process was precipitated as Ag_2S in
262 a trap containing 0.5 mL 1 M $AgNO_3$. Precipitated Ag_2S was then isolated by filtration, washed,
263 dried and weighed. Determination of the pyrite (FeS_2) content of the respective samples was
264 calculated by converting the weight of the precipitate (Ag_2S) to moles sulfur.

265

266 3.3 Push-pull test: Denitrification rate

267 The *in-situ* first order rate constant k of NO_3 reduction underneath the crop field was measured
268 using the single-well push-pull test method as described by Haggerty et al. (1998) and extended by
269 Yang et al. (2007). The principle is to derive the rate constant from the change over time in the
270 concentration of a reactive solute relative to a conservative solute tracer. Using a peristaltic pump,
271 ~15 L of groundwater from well TH32 was collected directly into a gas-tight aluminum bag, pre-
272 flushed in the field by N_2-gas to remove oxygen. 60 mL of an anoxic $NaNO_3$ and NaBr stock
273 solution was injected into the bag when half full (at ~7,5 L) using a syringe. When full, the bag was
274 carefully agitated to mix the solution inside it. The EC of the resulting mixed solution was
275 measured to ~700 µS/cm (twice the background EC of ~350 µS/cm) and a sample was withdrawn
276 to acquire the initial NO_3 and Br concentrations of 0.64 and 0.52 mM, respectively, before the
277 peristaltic pump was reversed to inject the solution back into 3 m depth. Recovery was conducted
278 28 hours later, during which EC was monitored; a total of 40 L water was withdrawn. During
279 recovery, ten water samples were collected covering a range of EC values, implying a range of
280 initial NO_3 concentrations. This enabled multi-point determination of the rate constant after the 28 h
281 reaction time and of its dependency on the initial NO_3 concentration.

282   The first-order rate constant k (positive for degradation) can be derived from (Yang et al. 2007,

283   Haggerty et al. 1998; after rearrangement):

$$kt = \ln\left(\frac{C_{tr}^{rel}(t)}{C_r^{rel}(t)}\right) + \ln\left(\frac{1 - e^{-kt_{inj}}}{kt_{inj}}\right) \qquad \text{Eq. 1}$$

284   where t is the time elapsed since injection ended and t_{inj} is the duration of the injection itself.

285    $C_{tr}^{rel}(t)$ and $C_r^{rel}(t)$ are the relative concentrations of, respectively, the tracer ($k = 0$) and the

286   reactive solute ($k \neq 0$), corrected for the respective background concentration (Yang et al. 2007):

$$C_{tr}^{rel}(t) = \frac{C_{tr}(t) - C_{tr}^b}{C_{tr}^{inj} - C_{tr}^b} \quad \text{and} \quad C_r^{rel}(t) = \frac{C_r(t) - C_r^b}{C_r^{inj} - C_r^b} \qquad \text{Eq. 2}$$

287   where C_{tr}^{inj} and C_r^{inj} are the injected (i.e., initial), and C_{tr}^b and C_r^b the background, tracer and

288   reactive solute concentrations, and $C_{tr}(t)$ and $C_r(t)$ are the tracer and reactive solute concentrations

289   of the samples taken during the test's 'pull' phase. The use of relative concentrations enables rate

290   determinations that do not depend on the fraction of injected-to-recovered amounts. In Eq. 1, the

291   second term on the right-hand side corrects for the *in-situ* reaction occurring during the test's

292   injection ('push') phase. In our case the duration of the injection was short (t_{inj}<1 h) relative to the

293    $t = 28$ h reaction time, which makes the right hand term in Eq. 1 insignificant (cf. Haggerty et al.

294   1998). Eq. 1 then becomes:

$$k = \ln\left(\frac{C_{tr}^{rel}(t)}{C_r^{rel}(t)}\right)/t \qquad \text{Eq. 3}$$

295   A first order rate constant k (h^{-1}) for each of the ten samples was calculated by applying Eq. 3 with

296   nitrate and bromide as the reactive and tracer solute, respectively; the average value is reported

297   here. The reaction timescale (τ_{react}) was subsequently calculated as (Ocampo et al. 2006):

$$\tau_{react} = \frac{1}{k} \qquad \text{Eq. 4}$$

298   The reaction timescale is comparable to the first-order reaction half-time $t_{\frac{1}{2}}$, as the two quantities

299   are separated only by a factor of $ln(2)$:

$$t_{\frac{1}{2}} = ln(2)\,\tau_{react} = 0.693\,\tau_{react} \qquad \text{Eq. 5}$$

300

301

302 3.4 Reactive transport modelling

303 The hydrochemical modelling software PHREEQC (Parkhurst and Appelo 2013) was used to

304 simulate the loss of nitrate with depth, observed in the shallow part of the aquifer under the crop

305 field. A one-dimensional (1D) reactive transport model with ten cells with a 1 m cell length was

306 defined (total 10 m depth). Assuming a vertical Darcy velocity of 0.5 m yr^{-1} (i.e., a 500 mm yr^{-1}

307 recharge rate) and a porosity of 0.3, the residence time of water in one cell (i.e., the time step) was

308 set to 0.6 yr (1.9×10^7 sec). A dispersivity of 0.1 m and an effective diffusion coefficient of $0.3 \times$

309 10^{-9} m^2 sec^{-1} were applied. For all cells (i.e., all depths), equilibrium with goethite and gibbsite was

310 defined, and pyrite and siderite were allowed to precipitate without being present from the start. The

311 database *phreeqc.dat* was used. The model was run for 50 shifts, corresponding to five flushes of

312 the complete 10-cell model, which ensured stationarity.

313

314 The model was calibrated by trial-and-error against observations from the multilevel profiles of

315 TH3, i.e., including its sister-piezometers TH32 and TH33. During calibration, the nitrate, oxygen

316 and Fe^{2+} concentrations of the recharging solution were adjusted, and amounts of organic carbon

317 (CH$_2$O) and pyrite were added to cells 1 to 5, individually, and allowed to react. Also, the goethite

318 stability (i.e., its equilibrium constant) was adjusted (same value used for all 10 cells). For the

319 infiltrating solution, representative values of sulfate (0.2 mM), pH (5.7), and alkalinity (0.6 meq/L)

320 were fixed.

321

322 Reacted amounts (of organic carbon or pyrite) ascribed to each cell of 1 m during fitting were

323 entered in units of mM and subsequently recalculated into rates in units of mM yr^{-1} by dividing by

324 the 0.6 yr residence time in the cell.
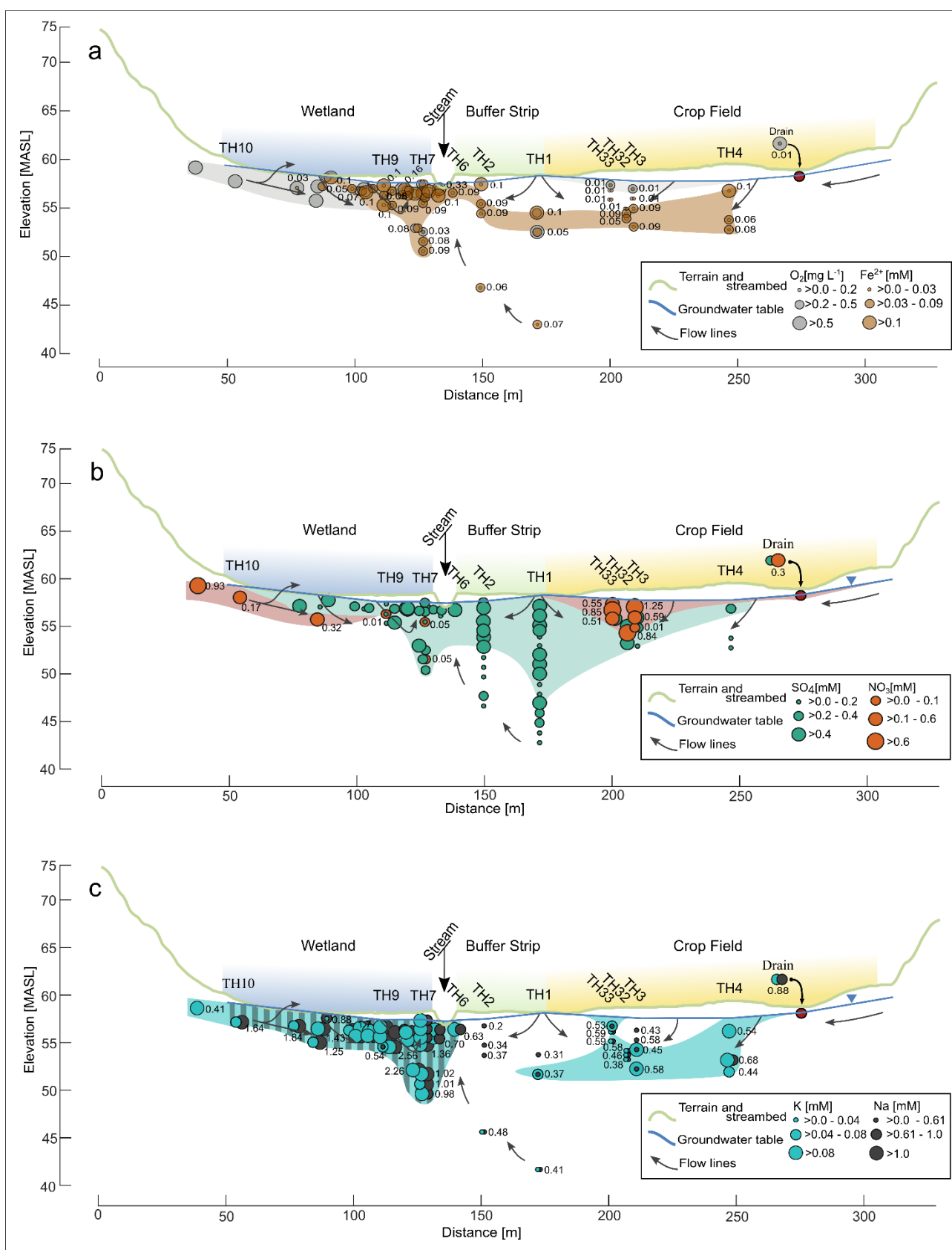
325

326 **4. Results**

327

328 The water chemistry is presented separately for groundwater and springs. First, key results from

329 groundwater sampled in piezometers across the entire stream valley are presented. This is followed

330 by the results from groundwater sampled from under the peat layer in the riparian wetland (using

331 mini-piezometers). Lastly, water chemistry from sampling of springs and stream water are

332 presented.

333

334 4.1 Groundwater chemistry (deeper piezometers)

335 Electrical conductivity (EC) in groundwater from the piezometers on the crop side of the stream

336 ranged from 179–400 μS cm^{-1}. TH3 and TH4 showed the highest EC. Groundwater below the

337 wetland had EC ranging from 271–524 μS cm^{-1}, slightly higher than at the crop side. The highest

338 EC was at TH10 located near the edge of the hillslope. Groundwater from TH8 had the lowest EC.

339 Higher EC values on the crop side of the stream were associated with higher concentrations of

340 calcium (Ca) and chloride (Cl). On the wetland side, higher EC were associated with higher

341 concentrations of Cl and sodium (Na, Figure 2C). Potassium (K) in groundwater below the wetland

342 had an average concentration of 0.13±0.05 mM (Figure 2C). Concentrations of K measured in

343 groundwater below the crop field were lower with an average of 0.04±0.03 mM, though elevated

344 potassium levels were seen in TH4, TH3 and TH33.

345

346 Dissolved oxygen (DO) in groundwater was low on both sides of the stream with the exception of

347 TH3 and TH10 (Figure 2A). On the crop side, only small amounts of DO were present in the

348 groundwater two MBS in TH3 (0.3 mg L^{-1}). From three MBS and deeper DO was <0.2 mg L^{-1}. In

349 addition, DO was found in groundwater at TH1s at depths of four and six MBS (0.4–0.7 mg O_2 L$^-$

350 ^{1}). Groundwater from TH10 showed DO concentrations of 1.4–2.2 mg O_2 L^{-1} indicating that

351 oxidized groundwater enters from the hillslope to the south. As groundwater moved closer to the

352 stream, DO decreased abruptly along the horizontal flow paths. In areas with low oxygen (anoxic

353 conditions) reduced iron (Fe^{2+}) or ferrous conditions were present (Figure 2A). Groundwater under

354 the crop field at 3–5 m depths had Fe^{2+} concentrations ranging from 0.01–0.1 mM. In groundwater

355 beneath the wetland, concentrations of Fe^{2+} ranged from 0.06–0.12 mM.

Figure 2. Cross-sections displaying concentrations of selected chemical components in groundwater collected from piezometers and 'mini'-piezometers. The interpreted flow field is from Steiness et al. (2019).

15

359   (a) Dissolved oxygen (grey, mg L^{-1}) and ferrous iron (Fe^{+2}) (brown, mM). Concentrations of Fe^{+2} in mM are

360   written next to data points. (b) Measured groundwater concentrations of Nitrate (red, mM) are also shown

361   next to data points and sulfate (green, mM). Samples with an ionic imbalance greater than 6% and less than

362   -6% have been excluded from the dataset. (c) Groundwater concentrations of potassium (turquoise, mM) and

363   sodium (black, mM) also written next to data points.

364

365   Nitrate was only present in groundwater at a few piezometers (Figure 2B). In TH3 and TH32 nitrate

366   concentrations were 1.2 and 0.6 mM, respectively at two and three MBS. From the hillslope to the

367   south, nitrate rich water enters the wetland and decreases to zero, along the horizontal flow paths

368   towards the stream (Figure 2B). Samples taken in March and November 2017 of groundwater from

369   TH10 had concentrations of 0.35 mM and 0.17 mM, respectively. Otherwise, groundwater samples

370   were to a large degree free of nitrate beneath the wetland. That is, samples of groundwater from

371   piezometers (TH7d, TH7s, TH9d, TH9s and TH8) in March had 0.0–0.05 mM and in November 0.0

372   mM. Groundwater samples collected from piezometer ST1 (screened 1.5 m below the streambed

373   just upstream of the ditch (Figure 1B), TH6 and TH8 (located approx. 1 and 1.5 meters from the

374   stream banks, respectively) contained no nitrate.

375

376   Sulfate (SO_4) concentrations in groundwater are shown in Figure 2B. Samples of groundwater from

377   TH3 and TH32 at three MBS, showed SO_4 concentrations of 1.3 and 1.9 mM, respectively. Closer

378   to the stream, groundwater from TH1s and TH2s had SO_4 concentration of 0.9–1 mM at 3–6 MBS,

379   similar to groundwater from TH3 and TH32. At depths of 6–8 MBS groundwater from TH1d

380   showed SO_4 concentrations of close to 1 mM. Concentrations of SO_4 were lower in groundwater

381   below the wetland with an average of 0.24 mM compared to an average of 0.4 mM on the crop side.

382   Concentrations >0.4 mM were found in groundwater located near the ditch (C10d, C20s and C20d).

383   The maximum concentration of 0.94 mM was measured in groundwater from C10d.

384

385   Alkalinity in groundwater ranged from 0.1–3.3 mM (data not shown). Groundwater from TH3 and

386   TH32 had the lowest alkalinities at 2–3 MBS ranging from ~0.1–0.4 mM. At four to six MBS, the

387   alkalinity in groundwater from TH3 was higher with concentrations of 1.5, 2.1 and 2.0 mM

388   respectively. In general, at depths of 2–8 MBS, alkalinity ranged from 0.7–1.9 mM. Groundwater

389   from the deepest piezometers, TH1d and TH2d, screened at 16 and 12 MBS, alkalinity was above

390   2.0 mM.

391   Groundwater below the wetland, closest to the peat, had alkalinity slightly higher than under the

392   crop field on the crop side of the stream. The highest alkalinity was measured in groundwater from

393   the two-piezometer nests TH7 (TH7s with 1.4–2.3 mM and TH7d with 3.1–3.3 mM) and TH9

394   (TH9s with 1.1–2.2 mM and TH9d with 1.1–1.7 mM).

395

396   4.2 Groundwater chemistry (shallow, wetland, mini-piezometers)

397   Samples collected from the shallow groundwater in the wetland using 'mini' piezometers had EC

398   ranging from 156–696 μS cm^{-1} (data not shown). Water from 'mini' piezometers P2 through P11

399   all had EC above 400 μS cm^{-1}. The highest EC was in P16 (561 μS cm^{-1}) and P19 (696 μS cm^{-1}).

400   Again, high EC was, as for the deeper groundwater below the wetland, mainly associated with

401   higher concentrations of Cl and Na. Likewise, concentrations of K was of the same magnitude as

402   for the deep groundwater under the wetland (mean 0.12±0.05 mM).

403

404   DO was present right below the peat layer near the hillslope. As groundwater flow closer to the

405   stream DO decreases abruptly (Figure 3A). Reduced iron (Fe^{2+}) ranged from 0.0–0.1 mM with an

406   average of 0.07 mM (data not shown). Inversely of the pattern of DO, alkalinity increased away

407   from the hillslope to the stream (Figure 3B). The increased alkalinity coincides with the location,

408   where the peat basin has its largest thickness (see Steiness et al. 2019).

409

410   NO_3 was present in high concentrations in shallow groundwater near the edge of the wetland, Figure

411   3C: P13 (0.32 mM), P16 (0.51 mM), P17 (0.93 mM), and P18 (0.06 mM). Closer to the stream

412   nitrate disappeared. Concentrations of SO_4 ranged from 0.0–0.75 mM (Figure 3D). High SO_4

413   concentrations were measured towards the ditch and the stream in P1, P2 and P3 near the stream,
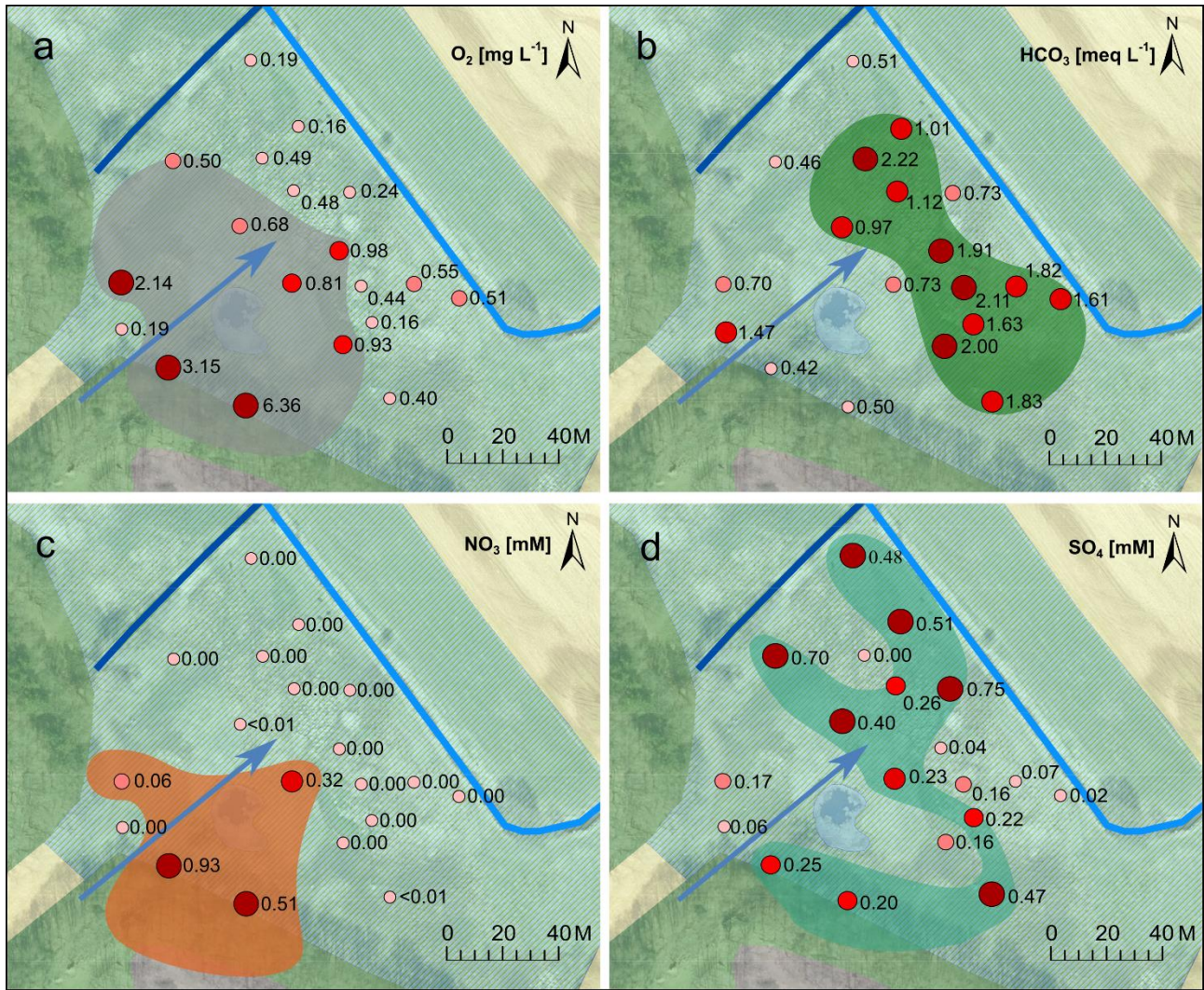
414   and P11 and P12 near the ditch.

Figure 3. Concentrations of (a) dissolved oxygen (mg L^{-1}), (b) alkalinity (meq L^{-1}), (c) nitrate (mM), and (d) sulfate (mM) of water samples taken of the shallow groundwater (~1 MBS) using mini-piezometers. Blue arrow indicates general direction of groundwater flow. Shadings indicate areas of elevated concentration.

4.3 Springs and stream

The EC of the six springs (DI, DW, PO, RI, S1 and S2) ranged from 334–575 µS cm^{-1}. The drainage well (DW) had the highest EC with an average of 502±54.5 µS cm^{-1}. The lowest EC was measured in PO and RI both with very similar average EC of 419 µS cm^{-1} and 417 µS cm^{-1}, respectively. The drain from the crop field had EC ranging from 253–361 µS cm^{-1}, which was very similar to the EC range measured in the stream (262–338 µS cm^{-1}). The chloride concentrations in the springs (average of 1.77±0.47 mM) were similar to chloride measured in the 'mini' piezometers. Concentrations of Cl in DI and DW were on average 2.19±0.44 mM and 2.45±0.51 mM,

18

428 respectively. These two springs had the highest measured Cl concentrations at the field site.

429 Potassium concentrations in the springs ranged from 0.04 mM to 0.27 mM, which was comparable

430 to K concentrations measured of both the deep and shallow groundwater on the wetland side.

431 Highest K concentrations were measured in PO and RI having mean K concentrations of 0.21 ± 0.03

432 mM and 0.17 ± 0.05 mM, respectively. Only S1 and S2 had concentrations of K <0.1 mM.

433

434 All samples taken from springs contain nitrate (NO_3) having a mean of 0.63 ± 0.14 mM and up to

435 0.97 mM, Figure 4. The highest concentration was measured in the water from the drainage well

436 (DW); ranging from 0.78 to 1.09 mM with an average of 0.8 mM. DI had the most variable NO_3

437 concentrations (0.39 to 0.94 mM). The second largest variation in NO_3 concentrations was observed

438 in DW. DW, S1 and S2 had similar temporal variations in NO_3, with the lowest concentrations in

439 the months of March and April 2017. A slight seasonality is observed in all springs. NO_3

440 concentrations in March and April show lower concentrations. Otherwise, seasonal variations in

441 NO_3 concentrations in the springs appear to be minor, e.g. only a slight decrease in concentrations

442 was seen over the summer.

443

444 Concentrations of NO_3 for the springs (DI, PO, DW, RI, S1, S2) were much higher than the NO_3

445 concentration of the stream (ST) and the drain (DR, draining parts of the crop field). NO_3 in the

446 stream (Figure 4) varied only slightly throughout the year, but with no apparent correlation to

447 stream discharge (Steiness et al, 2019). Stream nitrate concentrations were highest in February (0.12

448 mM), Nov. 2017 (0.13 mM) and Jan. 2018 (0.18 mM). The measured NO_3 concentrations from the

449 drain and the stream were very similar in both magnitude and timing, having the highest

450 concentrations during the late fall and winter.

451

452 Water samples taken from the submerged drain (Figure 1B) had an EC of 498 μS cm^{-1} and 520 μS

453 cm^{-1}, and contained 0.51 mM and 0.52 mM of NO_3; samples collected in May 2017 and January

454 2018, respectively. Potassium concentrations were 0.04 mM and 0.05 mM. EC, NO_3 and K

455 concentrations were very similar to what was measured in S2. In May 2017 and January 2018 S2

456 had an EC of 510 μS cm^{-1} and 474 μS cm^{-1} and NO_3 concentrations were 0.64 mM and 0.6 mM,

457 respectively. S2 had 0.05 mM of K in both May 2017 and January 2018, concentrations nearly

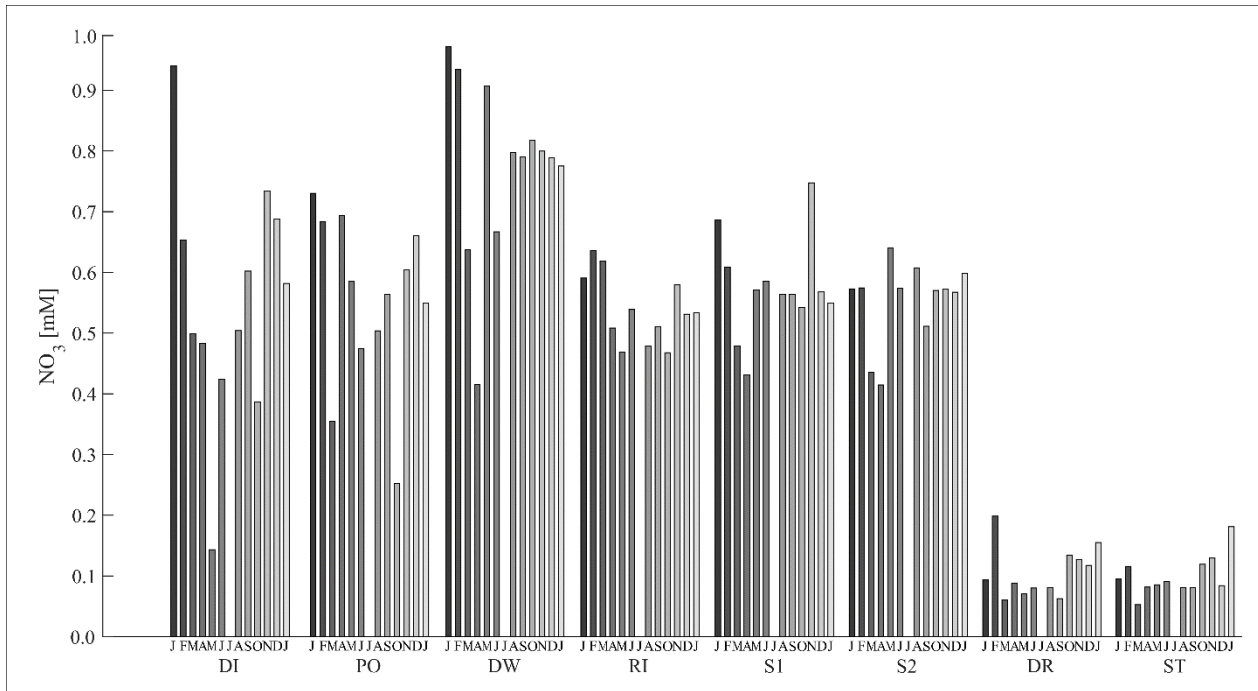458 identical to those of the submerged drain.

19

459

Figure 4. Nitrate concentration measured on a monthly basis from springs, the drain and stream. Month of measurement is given along the x-axis from January 2017 (dark grey) through January 2018 (light grey) (J, F, M, A, M, J, J, A, S, O, N, D, J).

4.4 Nitrate loads to stream

Figure 5 shows the calculated NO_3 load (kg N day^{-1}, concentrations from Figure 4) from the springs and submerged drain. Measured flow rates, converted to m^3/day, were taken from Steiness et al. (2019). Overall, the springs sustain a constant high N-input to the wetland surface and possibly to the stream. The highest nitrate loadings (kg N day^{-1}) were from S1 and RI mainly because the highest discharges were measured here (averaging 9.4×10^{-4} m^3 s^{-1} and 6.7×10^{-4} m^3 s^{-1}, respectively). Despite the similar nitrate concentrations at S2, S1 and RI, the lowest nitrate loading was from S2, due to a low discharge (average of 1.2×10^{-4} m^3 s^{-1}).

The combined average N-load from all springs was 708 kg N yr^{-1}. From DI and RI, both visibly discharging directly into the stream, the N-load was 219 kg N yr^{-1}. On the crop side of the stream an annual N-load to the stream from the drain, discharging directly into the stream, was 16.8 kg N yr^{-1}. The N-load from the springs was around 13 to 42 times higher than the N-load from the drain in the crop field. High N-loads from the springs S1 and RI are related to high water fluxes.
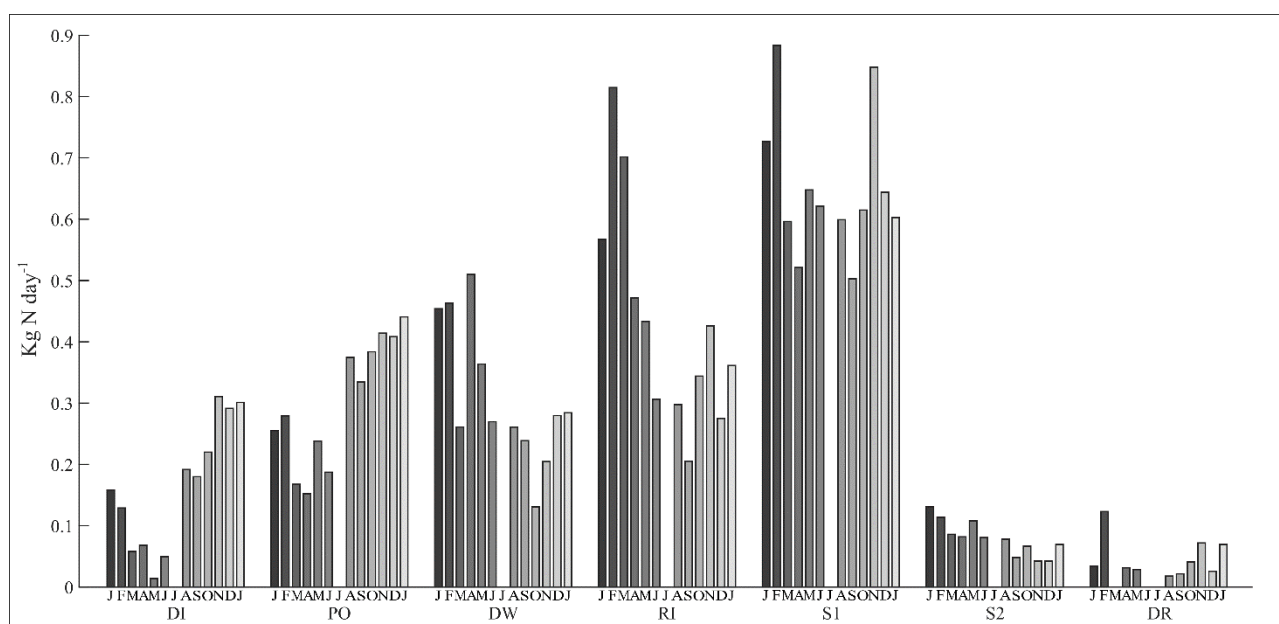
20

Figure 5. Nitrate loads calculated from concentrations and discharges measured on a monthly basis from the springs (DI, PO, DW, RI, S1, S2) and the drain (DR). Month of measurement is given along the x-axis from January 2017 (dark grey) through January 2018 (light grey) (J, F, M, A, M, J, J, A, S, O, N, D, J).

Samples collected in June 2017 from three ditches (D1, D2 and D3, Figure 1) downstream of the field site also showed high NO_3 concentrations. D1, D2 and D3 had 0.86, 0.99 and 0.38 mM of NO_3 respectively. The ditches had EC ranging from 245 to 290 µS cm^{-1} and chloride concentrations ranging from 0.62 to 0.82 mM. These were similar to the EC and Cl in the mini-piezometers. Mean potassium concentrations of water in the ditches were 0.11±0.02 mM.

4.5 Pyrite extraction

The core from 1.6 to 2.9 MBS was used for analysis of FeS_2. The sediment consisted of well-sorted sand with few pebbles. In the shallowest sample at 1.6 MBS, pyrite was not detected. Samples from 1.7, 1.8, 1.9 and 2.0 MBS contained, respectively, 1.5, 1.8, 2.0 and 1.9 mmol pyrite kg^{-1} dry sediment. The depth interval from 2.1–2.9 MBS was represented by a single mixed sediment sample; this sample had a pyrite content of 3.0 mmol kg^{-1} dry sediment.

4.6 Nitrate retention under the agricultural field

A push-pull test was conducted on 13–14 September 2016 at 3 m depth, within the anoxic zone, in well TH32. During installation of the well, the day before the push-pull test, the NO_3 concentration decreased with depth from 0.8 mM at 1.6 m depth to 0.08 mM at the 3 m test depth (i.e., background nitrate concentration), implying denitrification at the 3 m test depth; the background Br concentration at 3 m depth was 5.3 μM. In February 2016, a few meters from TH32, the NO_3 concentration likewise decreased from 1.2 mM at 1.9 m depth to 0.6 mM at 3.2 m depth, and was below the detection limit at 4.2 m depth. Application of Eq. 3 returned first-order rate constants (k) for nitrate reduction ranging from 1.5×10^{-2} to 0.68 d^{-1} (average 0.23 d^{-1}), corresponding to reaction timescales (τ_{react}) of ca. 1 to 66 days with a mean of 4 days.

4.7 Reactive transport modelling

Figure 6 shows the results of the reactive transport model (solid lines) and the observed chemical components from piezometers TH3, TH32 and TH33 (scatter points) located at the crop field. The observations showed that the most shallow samples of TH3, ~1.5−2 MBS or ~0.5−1 m below the groundwater table, contained up to 1.25 mM nitrate, but was anoxic (<0.25 mg O_2 L^{-1}) and ferrous (>0.4 mg Fe^{2+} L^{-1}). Just an additional 0.5−1 m deeper in the profile nitrate concentrations generally declined to below detection limit (Figure 6b). This suggests ongoing denitrification, which necessitated an even higher nitrate concentration in the recharge at the groundwater table. Accordingly, for the infiltrating solution in the model, a higher nitrate concentration of 2 mM was applied, together with an O_2 concentration of 0.3 mM (corresponding to saturation), and an Fe^{2+} concentration of zero.

Overall, the fit of the model results with the measured was satisfactory (Figure 6). The water table at TH3 (i.e., in Figure 6) was at 1 MBS. In the model, oxygen is depleted within the first 0.5 m below the water table (i.e., above 1.5 MBS) by reaction with organic carbon. This corresponds to an organic carbon reduction rate of 1.2 mmol C L^{-1} yr^{-1} in the most surficial part of the aquifer, where pyrite was not detected (cf. above). Deeper, where pyrite was detected, the model suggests NO_3 reduction exclusively by pyrite, with average nitrate reduction rates of 2.5 mmol NO_3 L^{-1} yr^{-1} between 1.5 and 2.5 MBS, decreasing to 0.6 mmol NO_3 L^{-1} yr^{-1} between 2.5 and 3.5 MBS, where

528   nitrate becomes depleted. The corresponding rates of pyrite oxidation are 0.9 and 0.2 mmol FeS_2

529   L^{-1} yr^{-1}, respectively. Between 1.5 and 2.5 MBS, the reaction is a complete oxidation of pyrite

530   followed by goethite precipitation:

531    $$5FeS_2 + 15NO_3^- + 5H_2O \rightarrow 5FeOOH + 10SO_4^{2-} + \frac{15}{2}N_2 + 5H^+ \tag{1}$$
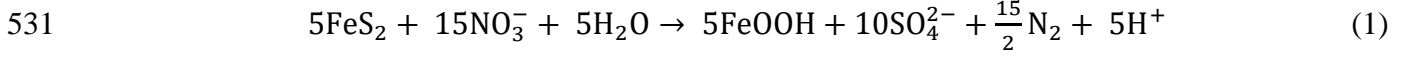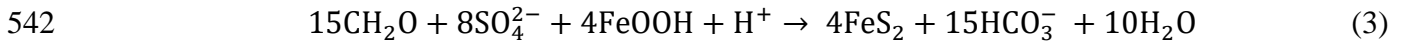
532   Consistent with this reaction, concentrations of SO_4 increased and decreases in pH and alkalinity

533   were observed, while, generally no or little concurrent release of ferrous iron occurred (Figure 6C –

534   F). Between 2.5 and 3.5 MBS the modelled denitrification occurred by incomplete pyrite oxidation:

535    $$5FeS_2 + 14NO_3^- + 4H^+ \rightarrow 5Fe^{2+} + 10SO_4^{2-} + 7N_2 + 2H_2O \tag{2}$$
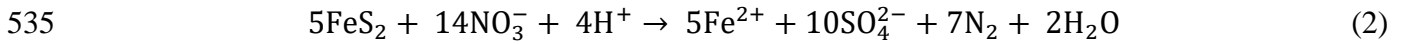
536   Contrary to reaction (1), reaction (2) releases Fe^{2+} and consumes protons, which is consistent with

537   observed increases in ferrous iron and pH over this depth interval.

538   Below 3.5 MBS, the model results suggested concurrent reduction of sulfate and iron oxides by

539   organic carbon oxidation followed by precipitation of pyrite (not shown in Figure 6). Here, the

540   ferrous iron removed from solution by pyrite precipitation is replaced by iron released by iron oxide

541   reduction, according to the overall reaction:

542    $$15CH_2O + 8SO_4^{2-} + 4FeOOH + H^+ \rightarrow 4FeS_2 + 15HCO_3^- + 10H_2O \tag{3}$$

543   This reaction is consistent with the observed removal of SO_4 from solution, increased alkalinity and

544   pH and invariable ferrous iron concentration below 3.5 MBS (Figure 6c–f). Concurrent sulfate and

545   iron oxide reduction (i.e., reaction (3)) is feasible for iron oxides that are slightly less stable than

546   goethite (Appelo and Postma, 2005). In line with this, the fitted saturation index of −0.4 for goethite

547   in the model was slightly negative. The simulated rate of organic carbon oxidation between 3.5 and

548   4.5 MBS was 4.8 mmol C L^{-1} yr^{-1}, dropping to 0.3 mmol C L^{-1} yr^{-1} from 4.5–5.5 MBS. In

549   summary, the reactive transport modelling substantiated that water chemistry observations

550   underneath the crop field are quantitatively consistent with, predominantly, denitrification by pyrite.
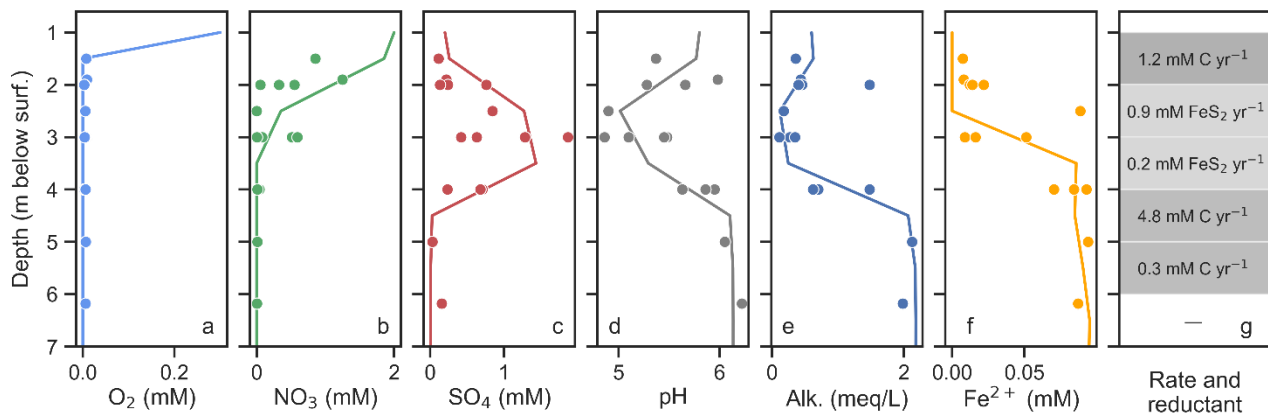
551

Figure 6. Measured (points) and modelled (lines) water chemistry in the aquifer below the crop field. The water table is at 1 MBS. Reactive transport modelling was conducted using PHREEQC-3.

5. Discussion

5.1 Nitrate distribution and removal processes in shallow groundwater

Nitrate was present in shallow groundwater beneath the crop field (TH3, TH32 and TH33) and in the water from the drainpipe. Nitrate was also found in the shallow groundwater along the hillslope in the wetland, where a shallow plume extends approximately 50 m into the wetland. On both sides of the stream, nitrate was removed in groundwater before it reached the stream via groundwater. Under the crop field, vertically infiltrating nitrate was removed a few meters below the groundwater table. Under the peat layer of the wetland nitrate was removed with horizontal flow towards the stream. Thus, groundwater samples taken immediately from below the streambed and from piezometers located near the stream bank contained no nitrate. Furthermore, samples from TH1 (to 16 m, Figure 2B) right at the border between the crop field and 35 m wide buffer zone contained no nitrate.

Oxygen (inhibiting denitrification) was present in groundwater arriving to the wetland from southwest, but near-anaerobic (DO <0.5 mg L^{-1}) and ferrous conditions were found at closer proximity to the stream, as well as everywhere under the crop field. Nitrate reduction in groundwater on the crop side was identified as occurring by denitrification. Reactive transport modelling suggests that nitrate was effectively removed a few meters below the water table by

24

575 autotrophic denitrification with pyrite (which was found to be present) in the top 1.5 m below the

576 groundwater table. The *in-situ* rate measurement (push-pull) and the reactive transport model agree

577 in suggesting complete reduction of a few mM nitrate within about a year. A successive production

578 and reduction of SO_4 along the groundwater flow paths results in a plume of elevated SO_4

579 concentrations at 3 to 8 MBS in the aquifer under the crop field (Figure 2B), which could be a

580 legacy of denitrification by pyrite (Jessen et al. 2017). However, the reactive transport model

581 (Figure 6) suggests that denitrification is followed by pyrite precipitation in some places (e.g., the

582 location of TH3), as SO_4 and iron oxides react with organic matter. Buried organic carbon in the

583 stream valley can originate from e.g. an old stream meander (Devito et al. 2000).

584

585 Postma et al. (1991) reported average sediment FeS_2 concentrations of 3.6 mmol kg^{-1} at a field site

586 situated 50 km north of the Holtum field site. In addition, they found FeS_2 to be the main electron

587 donor for O_2 and NO_3 reduction in the aquifer. Böhlke et al. (2002) also reported denitrification

588 coupled with reduced ferrous and sulfur compounds, including FeS_2. Both studies were conducted

589 within sandy outwash aquifers similar to our site. Sediment FeS_2 concentrations, below the water

590 table, were in this study 1.5–3.0 mmol kg^{-1}, likely sufficient for sustaining denitrification for many

591 decades (cf. Jessen et al. 2017). Nitrate discharge to the stream via groundwater from the crop side

592 could therefore continue to be low for many years. Recall, however, that a drain on the crop side

593 gives a load of 16.8 kg N yr^{-1} to the stream (Figure 5).

594

595 On the wetland side, sulfate concentrations in the shallow groundwater were at a few locations

596 similar to concentrations measured in the deeper groundwater. Sulfate concentrations in these areas

597 could be a legacy of "*hot spots*" for denitrification with reduced inorganic sulfur compounds.

598 Denitrification, though, could mainly be with organic matter perhaps as a result of infiltrating

599 dissolved organic matter from the peat layer. Denitrification with dissolved organic matter results in

600 an increased alkalinity (Figure 3B). A similar situation was found by Jensen et al. (2017), where a

601 top peat layer and 1–2 m below the peat layer were high-reactive zones. However, at a more

602 downstream site to ours, Karan et al. (2013) found high nitrate concentrations below a peat layer

603 and within the top five meters of a sandy aquifer across an entire riparian wetland. The wetland was

604 less dominated by springs and most of the regional flow input to the wetland and the stream was via

605   the conductive sandy aquifer with persistent aerobic conditions and, hence, limited nitrate reduction

606   potential.

607

608   According to the above, nitrate removal in water arriving as groundwater to the stream at our site

609   was found to be substantial and near 100%. Our results can be compared with the compilation of

610   field data in Ocampo et al. (2006), who evaluated nitrate removal efficiency (0–100%) from nine

611   field studies and compared these with a calculated Damköhler number (D), defined as:

$$D = \frac{\tau_{trans}}{\tau_{react}} \qquad \text{Eq. 6}$$

612   where τ_{trans} was computed as travel length divided by pore water velocity and τ_{react} is as defined

613   above. From Steiness et al. (2019) we obtain a hydraulic gradient of 0.01 and 0.02 towards the

614   stream from the hillslope north and south of the stream. With a mean hydraulic conductivity of 14

615   m/day (Steiness et al. 2019) and a porosity of 0.3, τ_{trans} is estimated to 75 and 310 days from the

616   start of the buffer zone and northern hillslope to the stream, respectively. On the wetland side,

617   τ_{trans} is 86 days from the southern hillslope to the stream. From the push-pull test we estimated a k

618   of 0.23 day^{-1} on the crop side based on denitrification with pyrite. On the wetland side,

619   denitrification is mostly like related to a reaction with dissolved organic matter. We have no

620   information of local denitrification rates with organic matter. Instead, we use information from a

621   similar site just downstream, where a maximum rate just below the peat layer was estimated to 0.25

622   day^{-1} (Ribas et al. 2017), i.e., very similar to the rate with pyrite denitrification. This gives D ~17–

623   71 and 21 on the crop and wetland sides, respectively. From Figure 10 in Ocampo et al. (2006) it is

624   clear that ~100% NO$_3$ removal occurs at D > 8–10. Bypass flows are therefore the main source of

625   N-loading to the stream.

626

627   5.2 Nitrate loading from springs and buffer efficiency

628   The upland to the crop field consist of coniferous forest so the main input of nitrate to groundwater

629   is the crop field. Hansen et al. (2012) estimated the regional annual agricultural N surplus in

630   Western Jutland in 2007 to 143 kg N ha^{-1} yr^{-1}. NO$_3$ leaching from the root zone have been reported

631   by Dalgaard et al. (2011) to amount to approx. 60% of the N-surplus for Danish conditions. The

632   crop field represents approx. 2 hectares giving potentially 172 kg N yr^{-1} leaching from crop field

633   due to application of N-fertilizers. Of this only 16 kg N yr^{-1} reaches the stream through the drain.

634   The crop side of the riparian lowland therefore has an N-removal efficiency of 90%. Consistently,

635   based on drain discharge measurements from Steiness et al. (2019) one can estimate that the bypass

636   flow to the stream from the drainpipe is approx. 10% of the total flow.

637

638   In the wetland, several groundwater-fed surface flows (bypass) with spring discharge together

639   contribute up to 59% of the stream flow gain (Steiness et al. 2019). The high nitrate concentrations

640   in the springs (Figure 3) result in a high N input to the wetland surface and eventually the stream. If

641   all springs contribute independently the N-load to the stream is 708 kg yr^{-1}, which must be

642   considered a maximum. If the spring contributions are not independent, so that the same nitrate was

643   measured multiple times and, effectively, only the ditch (DI) and the rivulet (RI) that visibly are

644   connected to the stream deliver nitrate to the stream, the resulting load of 218 kg N yr^{-1} by

645   groundwater-fed surface flow is still significant.

646

647   The upland southwest of the field site mainly consists of intensively farmed arable lands. Borehole

648   96.1981 from the national well database shows elevated nitrate concentrations to at least 20–30 m

649   below surface or 12–20 meters below the water table (Figure 1C). This suggests that there is little to

650   no reduction capacity (e.g., pyrite) at or above this depth in the aquifer. The regional groundwater

651   inflow to the wetland thus can have high nitrate concentrations, as confirmed by nitrate data from

652   TH10, the mini-piezometers, and springs.

653

654   Applying a simple analytical model, regional water- and N-fluxes were calculated (Appendix A).

655   The NO_3 concentrations from borehole 96.1981 were used as a baseline for the concentration of the

656   upland groundwater. This resulted in a water flux of 1955 L m^{-1} day^{-1} and an N-flux of 22–27.2 g

657   N m^{-1} day^{-1}. This further gives an annual regional N-load to the riparian wetland of 1033 kg N yr^{-1}

658   (average 1990-2008) and 1293 kg N yr^{-1} (year 2007). Steiness et al. (2019) reported a mean water

659   contribution from the wetland to the stream flow gain of 3.2×10^{-3} m^3 sec^{-1} in 2017, equal to 2130

660   L m^{-1} day^{-1}. Hence, there is a reasonable agreement (within 9%) of the two water fluxes. Hill

661   (2019) reported values of subsurface water- and N-fluxes to riparian buffers from several studies.

662   For sloping landscapes with sandy sediments, water fluxes were reported to range up to 1200 L m^{-1}

663 day^{-1} and N-fluxes of upwards of 26 g N m^{-1} day^{-1}. The water flux (1955 L m^{-1} day^{-1}) and N-load

664 (22–27.2 g N m^{-1} day^{-1}) to the riparian wetland are hence in the high end of reported fluxes.

665

666 The mean residence time from of regional discharge to the wetland is approximately 10 years

667 (Appendix A). As our data is from 2017, we now base the calculations on the N load using 2007

668 data from borehole 96.1981. As no nitrate enters the stream by groundwater, the N removal is

669 1293–708 = 585 kg N yr^{-1} or 450 kg N ha^{-1} yr^{-1} (wetland area of 1.3 ha). This is equivalent to a

670 buffer efficiency of 45%. These removal rates compare well with other studies conducted in Danish

671 riparian lowlands, located in Western Jutland, with N-removal capacities of 400 kg NO$_3$-N ha^{-1} yr^{-1}

672 (Brüsch and Nilsson 1993) and 119-340 kg NO$_3$-N ha^{-1} yr^{-1} (Hoffmann et al. 2006). A recent study

673 by Audet et al. (2020) on eight restored wetlands in Denmark reported lower removal rates of 42 kg

674 Total Nitrogen ha^{-1} yr^{-1}, with similar rates for NO$_3$, corresponding to buffer efficiencies between 2-

675 42%. These lower rates are in line with other studies listing removal rates of 9-70 kg NO$_3$-N ha^{-1}

676 yer^{-1} (Pärn et al. 2012) and 35-40 kg NO$_3$-N ha^{-1} yr^{-1} (Jensen et al. 2017).

677

678 These calculations were done assuming all springs contribute individually to the N load to the

679 stream. If we instead use the N load of 218 kg N yr^{-1} as measured from only DI and RI (the two

680 with visible outlets to the stream), the N loss is 1293–218 = 1075 kg N yr^{-1} (buffer efficiency of

681 83%). This is equivalent to 827 kg N ha^{-1} yr^{-1}, much higher than reported in other studies. If this

682 indeed was the case, re-infiltration of surface water in the wetland would prove to be an important

683 N-removal process. Revsbech et al. (2005) showed that nitrate concentrations in the water column

684 of a flooded meadow decreased exponentially by a τ_{react} of ~1 day, and re-infiltration and diffusion

685 could therefore be a substantial sink. Re-infiltration is supported by Steiness et al. (2019), who

686 observed a small downward gradient between TH9s and TH9d and enriched isotope values in

687 shallow groundwater in the center of the wetland. Re-infiltration was also found to be important by

688 Petersen et al. (2020).

689

690 In summary, the two sides (crop and wetland) show distinctly different characteristics. At first, one

691 would think that the crop field would be the main source of nitrate to the stream, but this is not the

692 case (except for the drain). This side of the stream is well protected by a redox front (pyrite) just a

few meters below the water table, a high crop field to upland area ratio (47%), and no nitrate source
in the upland. The regional inflow of groundwater is therefore low and bypass flow (10%) only
occurs as drain flow. On the wetland side, the wetland to upland ratio is very low (5%) giving a
relatively high inflow of groundwater. This groundwater has high nitrate concentrations, because of
the deep position of the redox front (12-20 m below the water table) in the regional aquifer
connecting to the wetland from southwest. Bypass flow is therefore significant (59%) on the
wetland side. Within the next one-two decades, the N-load via groundwater-fed surface flow on the
wetland side will likely decline, as the monitoring wells at the catchment boundary have shown a
decline in nitrate concentrations. For example, nitrate concentrations in well 96.1981 were 22-33%
lower in 2018 than in 2007.

The role of bypass flow containing high nitrate levels is not only limited to the field site. Several
ditches draining the wetland downstream of the field site were found to have high nitrate
concentrations. It appears that bypass flow via groundwater-fed surface flow plays an important role
in the delivery of nutrients along this section of Holtum stream. This may be due to the management
of the wetland, i.e., (i) channelization of the stream, (ii) installation of a drainage network, and (iii)
no maintenance of the drainage network resulting in broken drainpipes.

5.3 Implications – conceptual model

This section aims to compare the results of the detailed field study, as presented so far in this paper,
to synthetic cases. For this, we define the fraction of water passing a riparian lowland as bypass
flow f_{bypass}, and the fraction of diffuse flow through the riparian aquifer f_{diff}, and assume that
$f_{bypass} + f_{diff} = 1$. In our terminology, bypass flow therefore includes flow via subsurface drains,
rivulet-pipe flow (fast flow component, cf. Shabaga and Hill 2010), and diffuse surface flow (slow
flow component), the two latter ones being the result of groundwater-fed surface flow. We further
assume that no NO_3 degradation occurs along bypass flow paths, and that NO_3 removal in the
riparian aquifer follows the first-order rate law:

$$C_t = C_0 e^{-kt}$$ Eq. 7

where C_0 is the (initial, $t=0$) NO_3 concentration of water arriving to the riparian aquifer and C_t is the
concentration in water leaving the aquifer, after time t. This allows calculation of the overall NO_3

722 removal efficiency (fraction), i.e., the average concentration of NO_3 in all water arriving to a

723 riparian lowland (C_0) relative to that of all water leaving the lowland (C_{out}, equal to $f_{bypass}C_0 +$

724 $f_{diff}C_t$), by:

$$\text{Nitrate removal efficiency} = (1 - \frac{C_{out}}{C_0}) = 1 - f_{bypass} - f_{diff}e^{-kt} \qquad \text{Eq. 8}$$

725 Combining with the Damköhler number definition (Eq. 6), and realizing that time t in Eq. 7 and 8 is

726 equivalent to the travel time τ_{trans} in Eq. 4 yields:

$$(1 - \frac{C_{out}}{C_0}) = 1 - f_{bypass} - f_{diff}e^{-D} \qquad \text{Eq. 9}$$

727 Eq. 9 shows that the NO_3 removal efficiency is not a function of time per se, but is instead a

728 function of the time relative to reaction rate, as expressed by the Damköhler number. Further, the

729 removal efficiency depends on f_{bypass} (and therefore also on $f_{diff} = 1 - f_{bypass}$), and is

730 independent from the initial NO_3 concentration when first-order kinetics applies. Eq. 9 therefore

731 allows us to calculate very generically the NO_3 removal efficiency for any riparian lowland as a

732 function of bypass fraction and the riparian aquifer's Damköhler number. Accordingly, Figure 7

733 applies Eq. 9 to illustrate the effect on the NO_3 removal efficiency of the occurrence of bypass flow

734 across a riparian zone in combination with the denitrification rates (expressed as reaction

735 timescales, τ_{react}) and travel times (τ_{trans}) encountered within the riparian aquifer. In Fig. 7, the *x*-

736 axis indicates the percentage of bypass flow, and the *y*-axis shows a large range of Damköhler

737 numbers. As indicated above, flow paths in Figure 7 are assumed to have either an infinitely short

738 travel time, indicating bypass flow with no time for denitrification, or a long travel time, indicating

739 diffuse groundwater flow in the riparian aquifer. The color scale yields bluish colors when more

740 than 80% (i.e, >0.8) of the nitrate loaded to a riparian zone becomes reduced before water exits to

741 the stream.

742

743 Our field site's Damköhler numbers (derived above) for the two sides of the stream are

744 superimposed on Figure 7. On the agricultural side, only 10% of the water arrived to the stream as

745 bypass flow via the drain ($f_{bypass} = 0.1$), resulting in an overall removal efficiency above 90%. On

746 the wetland side, the high percentage of bypass flow (60–90%) keeps the overall nitrate removal

747 efficiency at less than ~40% at *any* Damköhler number, including, of course, the estimated value. In

748 other words, bypass flow completely controls the overall NO_3 removal efficiency. Such bypass flow

749 may occur via springs, rivulet-pipes, drains or ditches, or via the regional (non-riparian) aquifer
750 when it extends to beneath the stream.

751
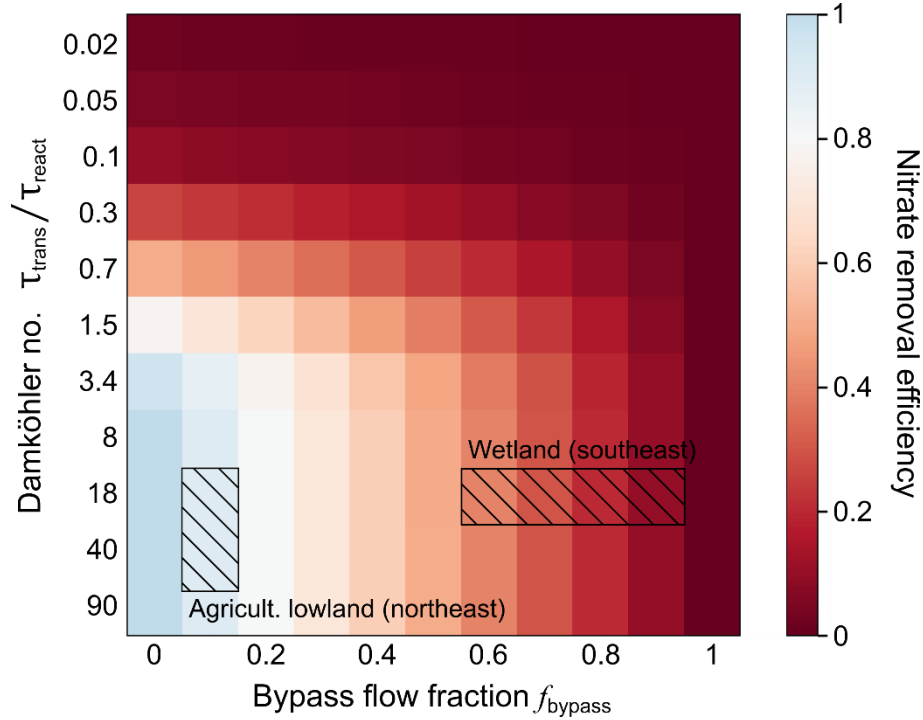
752 Figure 7. Nitrate removal efficiency as a function of the fraction of discharge that bypasses denitrification zones *vs.* the
753 Damköhler number, which reflects the transport time and first-order denitrification rate of the riparian aquifer.

754

755 Finally, we may extend Eq. 9 to also include degradation along the bypass flow, which necessitates
756 the definition of separate Damköhler numbers for the two flow paths:

$$(1 - \frac{C_{out}}{C_0}) = 1 - f_{bypass} e^{-D_{bypass}} - f_{diff} e^{-D_{diff}} \qquad \text{Eq. 10}$$

757 Degradation along the bypass flow paths could result from diffusion of labile organic carbon from
758 low-permeable peat strata into adjacent high-permeable zones of fast flow or into diffuse surface
759 flow path where flow is slower (Shabaga et al. 2010). Yet, for degradation along bypass flow paths
760 to be significant, denitrification rates along these flow paths need to by high as well, because of the
761 low residence times that characterizes bypass flow.

762

763

6. Conclusion

This study shows N-removal buffer efficiency of two riparian lowlands situated on opposite sides of a second order stream. Nitrate loading to the stream depended on the nitrate loading to, and redox conditions within, the regional aquifer, and on how groundwater arriving to the riparian aquifer was divided into bypass flow versus diffuse flow, representing different residence times and redox environments.

The riparian lowland with a crop field and a buffer zone situated to the northeast of the stream has a small upland with low water- and N-flux inputs. Despite the ongoing cultivation, only a small amount of nitrate-rich water was allowed rapid transition to the stream through a drainpipe. Nitrate in groundwater was effectively removed by autotrophic denitrification with pyrite in the aquifer under the crop field. Organic matter is believed also to be present (not measured) as reactive transport modelling suggests that SO_4 produced from pyrite oxidation is reduced by organic matter (shown by increase in alkalinity). Buffer efficiency was estimated to 90%.

The riparian wetland was connected to a five times larger upland dominated by arable lands and received both a high water- and N-flux. By appearance, the wetland represents a considerable potential for N-removal, but this potential is not fully realized. Groundwater-fed spring discharge as bypass flow ensured that nitrate-rich water could move rapidly across the riparian lowland to the stream. Clear signs of water table management, represented by old surface and subsurface drainage systems, are the causes of high fractions of bypass flow. The N-load to the stream is 708 kg N yr^{-1} if all springs individually contribute to the stream and 218 kg N yr^{-1} if only the two overland sources that directly discharge to the stream, i.e., a ditch and a rivulet, are accounted for. Compared to a calculated regional input of nitrate in 2007 (1293 kg N yr^{-1}) this gives buffer efficiencies of 45 and 83%, respectively. Thus, two conclusions arise; (1) if the total load to the stream is indeed 708 kg N yr^{-1}, then N-load to the stream is very high and buffer efficiency is rather low. (2) If the total load to the stream is indeed 218 kg N yr^{-1}, then surface re-infiltration to the peat layer and aquifer in the wetland is a significant process in N-removal.

The observation that bypass flow (drains, groundwater-fed surface flow) was important at this site resulted in the development of a conceptual model for nitrate removal efficiency as a function of the Damköhler number and the bypass fraction. The model requires information of a number of parameters such as estimates of the denitrification rates, groundwater velocity and the bypass fraction.

Water table management is a common practice conducted in riparian lowlands situated in agricultural lowland catchments. Reasons for the difference in N-removal efficiency can largely be attributed to vastly different external and internal factors. External factors include upland size (wetland-to-catchment area ratio), land use, and redox conditions in the upland aquifer, resulting in vastly different inputs across the upland-riparian interface. These factors are to a large degree magnified by the conditions met in the riparian zone; this is especially true for the riparian wetland, which is altered by anthropogenic changes affecting the subsurface and surface flow components to the streams. An improvement in the N-removal capacity would likely involve a rearrangement (restoration) of the entire stream valley. This would likely restrict the use of the stream valley with consequences for the current land use as productive agricultural land.

References

Audet, J., D. Zak, J. Bidstrup, and C.C. Hoffmann (2020). Nitrogen and phosporous retention in Danish restored wetlands. *Ambio* 49, 324-336.

Böhlke, J. K., R. Wanty, M. Tuttle, G. Delin and M. Landon (2002). Denitrification in the recharge area and discharge area of a transient agricultural nitrate plume in a glacial outwash sand aquifer, Minnesota. *Water Resources Research*, 38(7), 1105, 10.1029/2001WR000663.

821 Brüsch, W. and B. Nilsson (1993). Nitrate transformation and water movement in a wetland area.
822   *Hydrobiologica*, 251, 103-111.

823 Burt, T. P., L. S. Matchett, K. W. T. Goulding, C. P. Webster and N. E. Haycock (1999).
824   Denitrification in riparian buffer zones: the role of floodplain hydrology. *Hydrological*
825   *Processes*, 13(10): 1451-1463.

826 Burt, T. P., G. Pinay, F. E. Matheson, N. E. Haycock, A. Butturini, J. C. Clement, S. Danielescu, D.
827   J. Dowrick, M. M. Hefting, A. Hillbricht-Ilkowska and V. Maitre (2002). Water table
828   fluctuations in the riparian zone: comparative results from a pan-European experiment. *Journal*
829   *of Hydrology*, 265(1): 129-148.

830 Canfield, D. E., R. Raiswell, J. T. Westrich, C. M. Reaves and R. A. Berner (1986). The use of
831   chromium reduction in the analysis of reduced inorganic sulfur in sediments and shales.
832   *Chemical Geology* ,54(1): 149-155.

833 Clausen, J.C., K.G. Wayland, K.A. Saldi, and K. Guillard (1993). Movement of nitrogen through an
834   agricultural riparian zone: 1. Field studies. *Wat. Sci. Tech.*, 28(3-5): 605-612.

835 Cline, J. D. (1969). Spectrophotometric determination of hydrogen sulfide in natural waters.
836   *Limnology and Oceanography*, 14(3): 454-458.

837 Dahl, M., B. Nilsson, J. H. Langhoff and J. C. Refsgaard (2007). Review of classification systems
838   and new multi-scale typology of groundwater–surface water interaction. *Journal of Hydrology*,
839   344(1-2): 1-16.

840 Dalgaard, T., N. Hutchings, U. Dragosits, J. E. Olesen, C. Kjeldsen, J. L. Drouet and P. Cellier
841   (2011). Effects of farm heterogeneity and methods for upscaling on modelled nitrogen losses in
842   agricultural landscapes. *Environmental Pollution,* 159(11): 3183-3192.

843 Devito, K. J., D. Fitzgerald, A. R. Hill and R. Aravena (2000). Nitrate Dynamics in Relation to
844   Lithology and Hydrologic Flow Path in a River Riparian Zone. *Journal of Environmental*
845   *Quality*, 29(4): 1075-1084.

846 Haggerty, R., M. H. Schroth and J. D. Istok (1998). Simplified Method of "Push-Pull Test Data
847   Analysis for Determining In Situ Reaction Rate Coefficients. *Ground Water*, 36(2): 314-324.

848 Hansen, B., T. Dalgaard, L. Thorling, B. Sørensen and M. Erlandsen (2012). Regional analysis of
849   groundwater nitrate concentrations and trends in Denmark in regard to agricultural influence.
850   *Biogeosciences*, 9(8): 3277-3286.

851 Hefting, M., B. Beltman, D. Karssenberg, K. Rebel, M. Riessen and M. Spijker (2006). Water
852   Quality Dynamics and Hydrology in Nitrate Loaded Riparian Zones in the Netherlands.
853   *Environmental pollution*, 139: 143-156.

854 Hill, A. R. (1996). Nitrate Removal in Stream Riparian Zones. *Journal of Environmental Quality*,
855   25: 743-755.

856 Hill, A. R. (2018). Landscape Hydrogeology and its Influence on Patterns of Groundwater Flux and
857   Nitrate Removal Efficiency in Riparian Buffers. *Journal of the American Water Resources
858   Association*, 54(1): 240-254.

859 Hill, A. R. (2019). Groundwater nitrate removal in riparian buffer zones: a review of research
860   progress in the past 20 years. *Biogeochemistry*, 143(3), pp. 347-369.

861 Hoffmann, C., P. Berg, M. Dahl, S. Larsen, H. Andersen and B. Andersen (2006). Groundwater
862   Flow and Transport of Nutrients Through a Riparian Meadow – Field Data and Modelling.
863   *Journal of Hydrology*, 331: 315-335.

864 Jencso, K. G., B. L. McGlynn, M. N. Gooseff, S. M. Wondzell, K. E. Bencala and L. A. Marshall
865   (2009). Hydrologic connectivity between landscapes and streams: Transferring reach- and plot-
866   scale understanding to the catchment scale. *Water Resources Research*, 45, W04428,
867   doi:10.1029/2008WR007225.

868 Jensen, J. K., P. Engesgaard, A. R. Johnsen, V. Marti and B. Nilsson (2017). Hydrological mediated
869   denitrification in groundwater below a seasonal flooded restored riparian zone. *Water
870   Resources Research*, 53(3): 2074-2094.

871 Jessen, S., D. Postma, L. Thorling, S. Müller, J. Leskelä and P. Engesgaard (2017). Decadal
872   variations in groundwater quality: A legacy from nitrate leaching and denitrification by pyrite
873   in a sandy aquifer. *Water Resources Research*, 53(1), 184-198.

874 Karan, S., P. Engesgaard, M. C. Looms, T. Laier and J. Kazmierczak (2013). Groundwater flow and
875   mixing in a wetland–stream system: Field study and numerical modeling. *Journal of
876   Hydrology*, 488: 73-83.

877   Korom, S. F. (1992). Natural denitrification in the saturated zone: A review. *Water Resources*
878   *Research*, 28(6): 1657-1668.

879   Lutz, S. R., Trauth, N., Musolff, A., Van Breukelen, B. M., Knöller, K., and Fleckenstein, J. H.
880   (2020). How important is denitrification in riparian zones? Combining end-member mixing and
881   isotope modeling to quantify nitrate removal from riparian groundwater. *Water Resources*
882   *Research*, 56, e2019WR025528. https://doi.org/10.1029/2019WR025528

883   McClain, M. E., E. W. Boyer, C. L. Dent, S. E. Gergel, N. B. Grimm, P. M. Groffman, S. C. Hart,
884   J. W. Harvey, C. A. Johnston, E. Mayorga, W. H. McDowell and G. Pinay (2003).
885   Biogeochemical Hot Spots and Hot Moments at the Interface of Terrestrial and Aquatic
886   Ecosystems. *Ecosystems*, 6(4): 301-312.

887   Noij, I., M. Heinen, H. Heesmans, J. Thissen and P. Groenendijk (2012). Effectiveness of
888   Unfertilized Buff er Strips for Reducing Nitrogen Loads from Agricultural Lowland to Surface
889   Waters. *Journal of Environmental Quality*, 41: 322-333.

890   Ocampo, C.J., C.E. Oldham, M. Sivaplan, (2006), Nitrate attenuation in agricultural catchments:
891   Shifting balances between transport and reaction, *Water Resources Research*, 42, W01408,
892   doi:10.1029/2004WR003773

893   Parkhurst, D. and T. Appelo (2013). Description of input and examples for PHREEQC version 3-A
894   computer program for speciation, batch-reaction, one-dimensional transport, and inverse
895   geochemical calculations. U.S. Geological Survey Techniques and Methods, book 6, chap.
896   A43, 497 p., available only at https://pubs.usgs.gov/tm/06/a43/.

897   Pärn, J., G. Pinay, and Ü. Mander, (2012), Indicators of nutrients transport from agricultural
898   catchments under temperate climate: A review, *Ecological Indicators*, 22, 4–15,
899   doi:10.1016/j.ecolind.2011.10.002.

900   Peterjohn, W. T. and D. L. Correll (1984). Nutrient Dynamics in an Agricultural Watershed:
901   Observations on the Role of A Riparian Forest. *Ecolog,* 65(5): 1466-1475.

902   Postma, D., C. Boesen, H. Kristiansen and F. Larsen (1991). Nitrate Reduction in an Unconfined
903   Sandy Aquifer: Water Chemistry, Reduction Processes, and Geochemical Modeling. *Water*
904   *Resources Research;* 27(8): 2027-2045.

905   Poulsen, J. R., E. Sebok, C. Duque, D. Tetzlaff and P. K. Engesgaard (2015). Detecting
906   groundwater discharge dynamics from point-to-catchment scale in a lowland stream:

907 combining hydraulic and tracer methods. *Hydrology and Earth System Sciences*, 19(4): 1871-
908 1886.

909 Puckett, L. (2004). Hydrogeologic controls on the transport and fate of nitrate in ground water
910 beneath riparian buffer zones: Results from thirteen studies across the United States. *Water*
911 *science and technology*, 49(3), 47-53.

912 Puckett, L. and T. Cowdery (2002). Transport and fate of nitrate in a glacial outwash aquifer in
913 relation to ground water age, land use practices, and redox processes. J*ournal of Environmental*
914 *Quality*, 31: 782-796.

915 Puckett, L. and W. Hughes (2005). Transport and Fate of Nitrate and Pesticides: Hydrogeology and
916 Riparian Zone Processes. *Journal of Environmental Quality*, 34: 2278-2292.

917 Puckett, L. J. and W. B. Hughes (2005). Transport and Fate of Nitrate and Pesticides The use of
918 trade names in this paper is for identification purposes only and does not constitute
919 endorsement by the U.S. Geological Survey. *Journal of Environmental Quality*, 34(6): 2278-
920 2292.

921 Revsbech, N., J. Jacobsen and L. P. Nielsen (2005). Nitrogen transformations in microenvironments
922 of river beds and riparian zones. *Ecological Engineering*, 24: 447-455.

923 Ribas, D., M. Calderer, V. Marti, A.R. Johnsen, J. Aamand, B. Nilsson, J.K. Jensen, P. Engesgaard,
924 and C. Morici (2017), Subsurface reduction under wetlands takes place in narrow superficial
925 zones, *Environmental Technology*, DOI:10.1080/09593330.2016.1276220

926 Sabater, S., A. Butturini, J.-C. Clement, T. Burt, D. Dowrick, M. Hefting, V. Matre, G. Pinay, C.
927 Postolache, M. Rzepecki and F. Sabater (2003). Nitrogen Removal by Riparian Buffers along a
928 European Climatic Gradient: Patterns and Factors of Variation. *Ecosystems*, 6(1): 0020-0030.

929 Sebok, E., J. C. Refsgaard, J. J. Warmink, S. Stisen and K. H. Jensen (2016). Using expert
930 elicitation to quantify catchment water balances and their uncertainties. *Water Resources*
931 *Research*, 52(7): 5111-5131.

932 Shabaga, J. A. and A. R. Hill (2010). Groundwater-fed surface flow path hydrodynamics and nitrate
933 removal in three riparian zones in southern Ontario, Canada. *Journal of Hydrology*, 388(1-2):
934 52-64.

935   Steiness, Jessen, Spitilli, v. t. Veen, Højberg and Engesgaard (2019). The Role of Management of

936   Stream–Riparian Zones on Subsurface–Surface Flow Components. *Water*, 11: 1905,

937   doi:10.3390/w11091905

938   Stookey, L. L. (1970). Ferrozine---a new spectrophotometric reagent for iron. *Analytical Chemistry*,

939   42(7): 779-781.

940   Sweeney, B.W., and J.D. Newbold (2014), Streamside forest buffer width needed to protect stream

941   water quality, habitat, and organisms: A literature review, *Journal American Water Resource*

942   *Association*, 50(3), 560-584, DOI: 10.1111/jawr.12203.

943   Vidon, P. and A. R. Hill (2005). Denitrification and patterns of electron donors and acceptors in

944   eight riparian zones with contrasting hydrogeology. *Biogeochemistry*, 71(2): 259-283.

945   Vidon, P. G. F. and A. R. Hill (2004). Landscape controls on the hydrology of stream riparian

946   zones. *Journal of Hydrology*, 292(1-4): 210-228.

947   Yang, C., M. Park and C. Zhu (2007). A method for estimating in situ reaction rates from push-pull

948   experiments for arbitrary solute background concentrations. *Environmental and Engineering*

949   *Geoscience*, 13(4): 345-354.

Appendix A

Upland-riparian groundwater water- and N-flux calculation

Approx. 2000 m southwest of TH10 borehole 96.1981 is located, screened at two depths. The well is located near the topographic divide of the catchment. Well 96.1981 shows high nitrate concentrations in groundwater at depths 20-35 MBS. This suggests that nitrate reduction in the upland aquifer is poor. The water table and water flux from borehole 96.1981 to piezometer TH10 was calculated using an analytical model. A conceptualization of the simplified unconfined aquifer is presented in figure A.1.
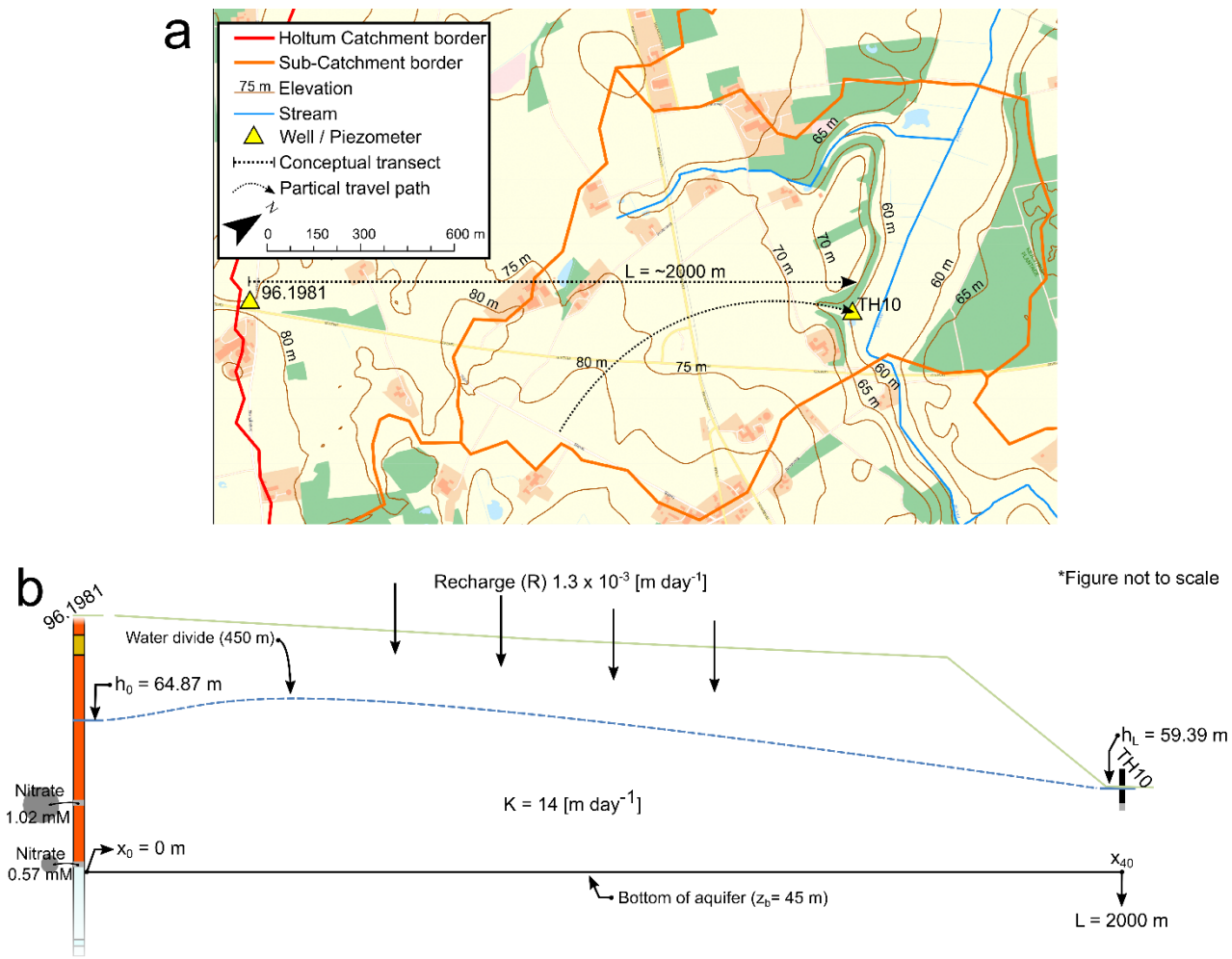
Figure A.1 Borehole 96.1981 from the national well database (Jupiter, GEUS) are located at approx. 2000 m from TH10. a) An overview of the location of the two wells used for the analytical model. Borehole 96.1981 is located just east of the Holtum Catchment border; approx. 600 m (northeast) from the borehole is the topographical water divide. b) Conceptual representation of analytical model to calculate water flux and N-load from upland (southwest) to riparian

963   wetland. Borehole 96.1981 are located at (x_0) 0 m and piezometer TH10 in the riparian wetland at (L and x_{40}) 2000

964   m. The aquifer has a saturated thickness ($h(x_n) - z_b$) assuming an aquifer bottom at 45 m. The hydraulic conductivity

965   (K) is 14 m day^{-1}, equal to the measured average K at the field site (Steiness et al. 2019). Recharge was mean annual

966   precipitation minus the mean annual actual evapotranspiration (Sebok et al. 2016). Figure not to scale.

967

968   The unconfined aquifer receives recharge (R) equal to the mean annual precipitation minus actual

969   evapotranspiration for Holtum catchment reported by Sebok et al. (2016). Borehole 96.1981 is

970   situated at x_0 (0 m) having a hydraulic head h_0 (64.87 m, see figure B.1). At the opposite end,

971   piezometer TH10 is located at 2000 m with a hydraulic head of h_L (59.39 m). An impermeable

972   bottom is assumed at elevation z_b (45 m). The saturated thickness is equal to $h(x) - z_b$. A 1D

973   steady state flow equation for an unconfined aquifer was used to calculate the head distribution h(x)

974   and flux q(x) (in units of m^3 day^{-1} per meter wetland;

975   *(A.2)*
$$h(x) = \sqrt{(h_0 - z_b)^2 + \frac{R}{K}(Lx - x^2) + \frac{(h_L - z_b)^2 - (h_0 - z_b)^2}{L}x} + z_b$$

976   *(A.2)*
$$q(x) = -\frac{K}{2}\left(\frac{R}{K}(-2x + L) + \frac{(h_L - z_b)^2 - (h_0 - z_b)^2}{L}\right)$$

977   The head distribution is shown in the conceptual model, Figure A.1. A water divide is predicted

978   approximately 450 m from 96.1981. This simple model therefore confirms that the well is located

979   near the topographic divide as seen in Figure A.1A.

980   The calculated $q_{L=2000\,m}$ at the entrance to the wetland is 1.96 m^3 day^{-1} m^{-1}. With a wetland width

981   of 130 m along the hillslope-riparian wetland interface at the field site, this yields an upland to

982   riparian wetland groundwater flux of 252 m^3 day^{-1} or 2.9 x 10^{-3} m^3 sec^{-1}. In comparison, Steiness et

983   al. (2019) measured a mean contribution from the southwest to the stream flow gain of 3.2 x 10^{-3} m^3

984   sec^{-1} (4.58×10^{-3} m^3 sec^{-1} x 0.7). The velocity-weighted average residence time was calculated to

985   ~10 years from the simulated water divide at 450 m to the entrance to the wetland at 2000 m

986   (assuming a porosity of 0.3).

987   Borehole 96.1981 has two filters where nitrate concentrations are measured on a regular basis

988   (yearly) as part of the national groundwater-monitoring program (Figure A.1). The average NO$_3$

989   concentrations over the period 1990-2018 were 1.02 mM and 0.57 mM for the top and bottom filter,

990   respectively. With an average residence time of about 10 years the nitrate input to the wetland could

991   also be estimated from what was measured in 2007 (10 years before the current investigation). The

992   2007 concentrations were somewhat higher with 1.39 mM and 0.6 mM in the top and bottom filters,

993 respectively. Three other monitoring wells are also present in the vicinity of well 96.1981. They all

994 have similar concentration ranges.

995 The N-load from upland to riparian wetland was calculated based on the average (1990-2018) and

996 2007 nitrate concentrations (C) from borehole 96.1981 times the groundwater-riparian wetland flux.

997   (A.2) $N_{load} = q_{L=2000\,m} \cdot C$

998 The regional N-load yields an input of 22-27.2 g N day^{-1} m^{-1}giving an annual regional N-flux of

999 1033-1293 kg N yr^{-1} with a wetland width of 130 m.